Uplift of the western Altiplano plateau: Evidence from the Precordillera between 20° and 21°S (northern Chile)

Pia Victor

Institut für Geologie, Universität Hannover, Hannover, Germany

Onno Oncken and Johannes Glodny

GeoForschungsZentrum Potsdam, Potsdam, Germany

Received 14 March 2003; revised 18 December 2003; accepted 3 February 2004; published 22 July 2004.

[1] We present a quantitative reconstruction of uplift of the western flank of the Altiplano plateau (central Andes), one of the largest monoclines on the Earth, on the basis of an analysis of tectonic structures, syntectonic deposits, and geophysical data. Uplift occurred on a west vergent, slowly propagating system of high-angle reverse faults merging into a joint detachment that ramps down to midcrustal levels below the plateau edge. The upper ramps determine local fold geometries while the lower ramp controls large-scale surface tilting and uplift. At 20°S, this fault system was active between ~30 Ma and 5–10 Ma, with maximum shortening rates of 0.22 mm/yr between 17 and 10 Ma. It generated some 2600 m of surface uplift with only minor shortening of ~3000 m. Its activity was largely synchronous to eruption of large-volume ignimbrites from a midcrustal source. Geophysical data indicate that the fault system localized deformation at the boundary between a cool, strong forearc crust and a presumably fluid-rich and/or partially molten zone underneath the plateau area. The systematic relation between crustal melting and shortening with uplift at the western plateau margin can be traced along most of the plateau flank, with a stepwise decrease in age of deformation and magmatism toward the south indicating discontinuous addition of plateau segments. Crustal thickening to as much as 70 km from westward underthrusting in the back arc parts of the plateau isostatically compensated the tectonic surface uplift and monocline formation with respect to a stable forearc, which only reacted with minor tilting. *INDEX TERMS:* 1035 Geochemistry: Geochronology; 8107 Tectonophysics: Continental neotectonics; 8015 Structural Geology: Local crustal structure; 9360 Information Related to Geographic Region: South America; 9604 Information Related to Geologic Time: Cenozoic; *KEYWORDS:* Andes, plateau formation. **Citation:** Victor, P., O. Oncken, and J. Glodny (2004), Uplift of the western Altiplano plateau: Evidence from the Precordillera between 20° and 21°S (northern Chile), *Tectonics*, *23*, TC4004, doi:10.1029/2003TC001519.

0278-7407/04/2003TC001519

1. Introduction

[2] Although oceanic subduction under the South American continent has been active since at least the Jurassic, the present day Andean Cordillera has largely formed during the last 30 Myr, synchronous to a stage of fast subduction of the Nazca plate under South America [e.g., *Isacks*, 1988; *Pardo-Casas and Molnar*, 1987; *Allmendinger et al.*, 1997; *Somoza*, 1998]. The resultant central Andes have developed a ~4 km high plateau that shows a remarkable topographic asymmetry with a steep monocline in the west versus a low-tapered margin in the east (Figures 1a and 1b). Formation and uplift of the plateau are widely considered the isostatic response to crustal shortening with thickening to as much as 60–80 km below the Altiplano [*James*, 1971; *Isacks*, 1988; *Wigger et al.*, 1994; *Zandt et al.*, 1994; *Beck et al.*, 1996; *Yuan et al.*, 2000]. Most of this shortening, however, has been accumulated at the eastern plateau flank, in the Eastern Cordillera and the Subandean fold and thrust belt, where the highest shortening rates with crustal scale west directed underthrusting are currently observed [*Baby et al.*, 1997; *Gubbels et al.*, 1993; *Allmendinger et al.*, 1997; *Lamb et al.*, 1997; *Kley and Monaldi*, 1998].

[3] As opposed to the fold-thrust belt nature of the eastern plateau margin, the western plateau margin forms a huge monocline that lacks prominent Neogene deformation structures. The monocline links the Longitudinal Valley, a continental forearc basin at 1000 m altitude, over a distance of some 50 km with the western plateau margin at an altitude of 4000–5800 m. This margin is formed by the Chilean Precordillera and the recent magmatic arc (Western Cordillera, Figure 1a). Despite its enormous size and N–S elongation of more than 800 km, the geodynamic nature of this monocline has attracted considerably less attention than its eastern counterpart. This is largely due to widespread cover of the monocline by young deposits evolved in a hyperarid climate, to a lack of obvious structures, and to scarce geophysical data imaging the subsurface.

[4] The discussion on the nature of the monocline is controversial. *Isacks* [1988] has suggested that uplift of this margin was the result of flexure of the crust as a response to late Miocene underthrusting from the east. More recently, *Muñoz and Charrier* [1996], *Farias et al.* [2002], and

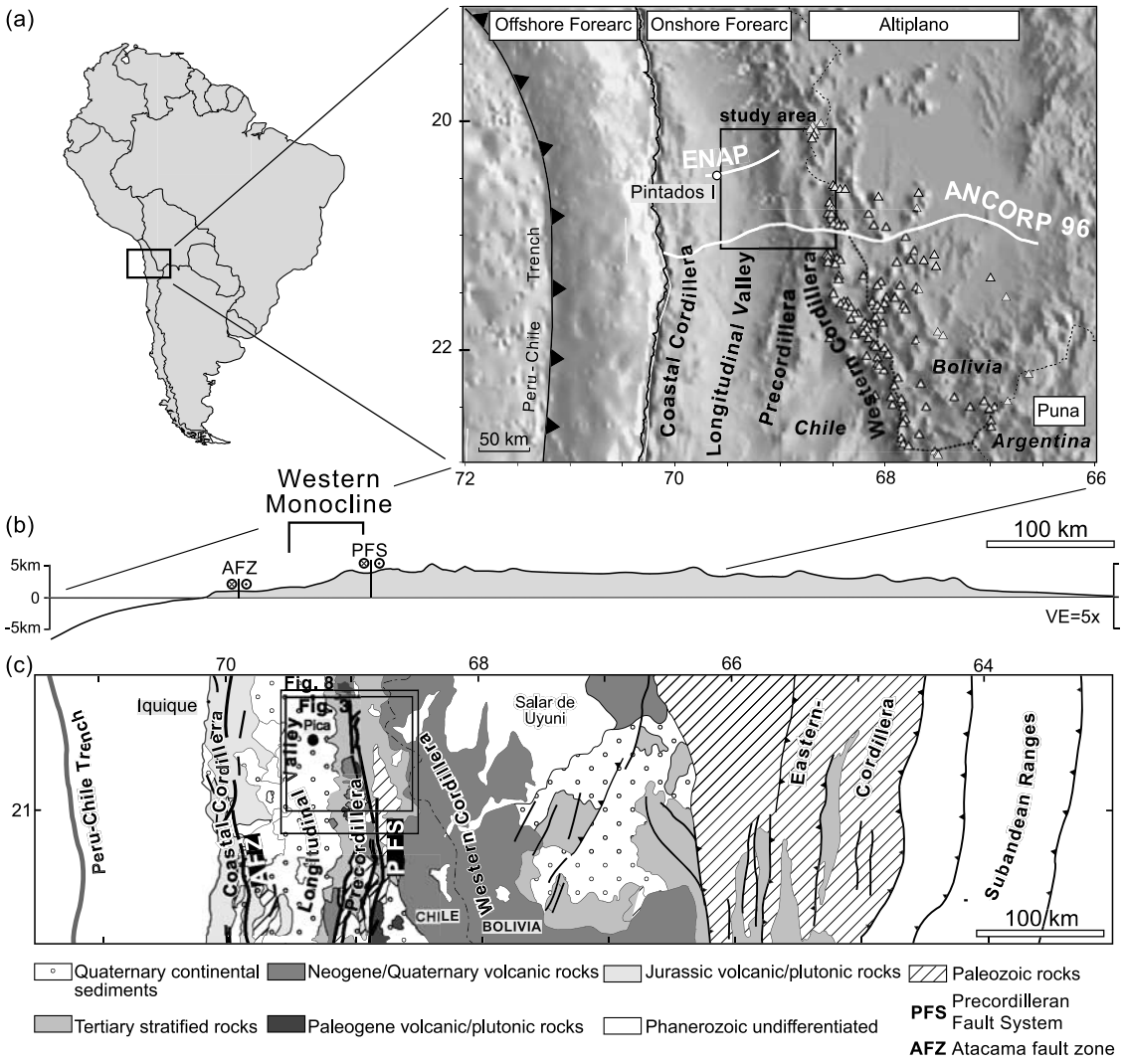

Figure 1. (a) Topography of the central Andean forearc and western Altiplano based on the GTOPO30 data set: Locations of seismic lines by ENAP, ANCORP'96 in the study area are displayed. (b) Topographic cross section through the central Andes at 21°S showing the Western Monocline. (c) Geological map of the 20°–22°S section of the central Andes depicting structural subdivisions, major faults in the forearc and back arc (AFZ: Atacama Fault Zone; PFS: Precordilleran Fault System; based on *Reutter et al.* [1994]).

García et al. [2002] have reported the occurrence of steeply east dipping reverse faults with low shortening magnitudes at the base of the monocline between 18°30′ and 19°30′S that they dated to be Miocene in age. They accordingly suggested a thrust-related uplift of the western Altiplano crust paralleled by surface tilting from deep-seated processes (cf. similar interpretations north and south by *Sébrier et al.* [1988] and *Muñoz et al.* [2002]). *Lamb et al.* [1997] explained the monocline as a gigantic tilted block of upper crust that collapsed and rotated between the subvertical Atacama and Precordilleran Fault Systems during Plio-Pleistocene plateau uplift. On a smaller scale, *Wörner et al.* [2000] describe similar large-scale antithetic block rotations at 18°S induced by gravitational collapse of the plateau flank (see, however, controversial discussion by *García and Hérail* [2001]). In addition, deformation of parts of the forearc has been shown to be dominated by vertical axis block rotations that have been either attributed to oroclinal bending of the Andes [*Isacks*, 1988; *MacFadden et al.*, 1995; *Kuhn*, 2002] or to oblique subduction during the Cenozoic [*Beck*, 1988; *Randall et al.*, 1996].

[5] In summary, the specific uplift mechanism and history of the western Altiplano plateau are subject of debate. Their reconstruction, however, may shed light on several of the main plateau-related issues: its formation mechanism, timing of uplift, and the relationship between tectonic and magmatic processes in plateau building. The present paper attempts to explore these aspects through a joint reconstruction of the structural, magmatic, and sedimentary evolution of this part of the plateau. Our analysis focuses on the area

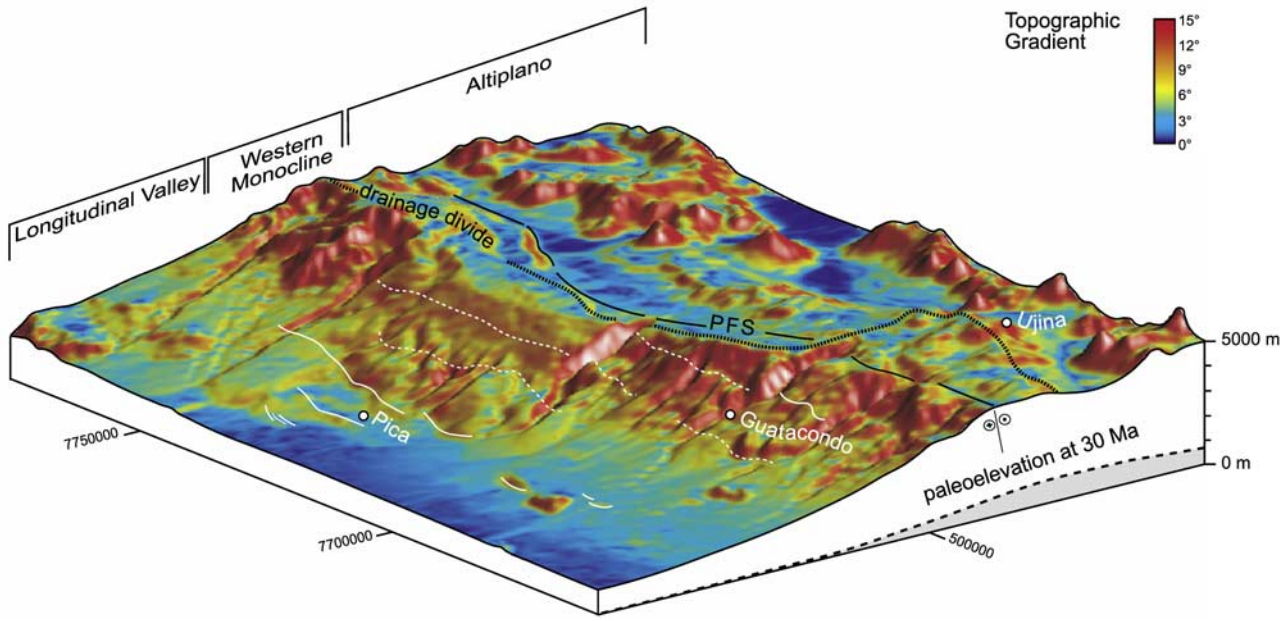

Figure 2. Perspective view of the study area showing the topography of the Western Monocline between ~20° and 21°S. Color coding corresponds to slope angles. Relatively high slope angles show a significant correlation with buried faults outlined with white solid (mapped) or white stippled (interpolated) lines. Assumed subdued topography at 30 Ma is shown as paleoelevation (see text). PFS, Precordilleran fault system.

at 20°–21°S (Figure 1a) for two reasons: (1) A recent series of geophysical observations at this latitude from the Berlin-Potsdam Andes group [*ANCORP Working Group*, 1999, 2003; *Yuan et al.*, 2000] and industry reflection lines yield the first complete deep image of the western plateau margin. (2) In this area, the Cenozoic volcano-sedimentary cover of the basement is preserved all the way from the Longitudinal Valley to the plateau top, which allows quantifying processes at high resolution. Although the area is small in extent, the findings in conjunction with published results permit us to draw general conclusions on the evolution of the entire western Altiplano plateau flank.

2. Regional Geomorphology and Geology

[6] On its western margin, the Altiplano encompasses the Chilean Precordillera and the recent magmatic arc (Western Cordillera), which has been active since ~28 Ma [*Baker and Francis*, 1978; *Coira et al.*, 1982; *Scheuber and Reutter*, 1992]. The Precordillera marks the western edge of the plateau with its crest line at an average elevation of 4200 m (Figures 1a, 1b, and 2). The crest position roughly coincides with the important Precordilleran fault system (PFS) and the axis of the Late Cretaceous-Paleogene magmatic arc. West of the Precordillera, the western flank of the Altiplano drops to an average elevation of 1000 m in the Longitudinal Valley (surface slope between 3° and 11°, diminishing down slope). This nearly flat sedimentary basin parallels the entire western flank separating the latter from the 1200 to 3000 m high Coastal Cordillera. At the spectacular coastal escarpment of more than 1000 m altitude, the Coastal Cordillera breaks off toward the coastline. Because of progressive aridity since the Miocene to the present hyperarid state [*Alpers and Brimhall*, 1988; *Gaupp et al.*, 1999], there was very little late Miocene to recent erosion in the entire area and geomorphic features related to deformation are nearly perfectly preserved. According to these landforms, deformation in the entire forearc is minor and shows a complex pattern involving deformation partitioning at several scales.

[7] The geological evolution of the forearc has been governed by eastward migration of the volcanic front from the Jurassic position in the Coastal Cordillera to its present position in the Western Cordillera. This migration has been interpreted to indicate tectonic erosion and subduction of more than 200 km of continental crust in a W-E section [*Rutland*, 1971; *Scheuber et al.*, 1994]. The migration was accompanied by an equally migrating zone of underplated mafic crust at or near the crust-mantle boundary, and intrusion into, the overlying crust [*Haschke et al.*, 2002]. The forearc crust is mainly built from Paleozoic basement rocks intruded and overlain by Mesozoic to Tertiary magmatic rocks from the various arc stages intercalated with marine and continental sediments (Figure 1c).

[8] Most deformation of the Precordillera and the forearc is Paleogene and older in age and is related to major subvertical strike-slip fault systems that originally developed as oblique contractional structures in the various magmatic arc segments (Precordilleran fault system [*Scheuber and Reutter*, 1992; *Reutter et al.*, 1996; *Tomlinson*

and Blanco, 1997]; Atacama fault system [*Scheuber and Andriessen*, 1990; *Reijs and McClay*, 1998; *Scheuber and Gonzalez*, 1999]). They were recently reactivated with transtensional kinematics and some vertical axis block rotations with a clockwise sense [*Randall et al.*, 1996; *Kuhn*, 2002]. Late Cenozoic plateau evolution, therefore, encountered a forearc largely controlled by magmatic rocks that intruded into, or overlie, deformed sediments and a heterogeneous continental basement.

3. Stratigraphy

[9] On top of a regional unconformity, Oligocene to Quaternary continental clastic sediments and volcanic rocks of up to 1000–1500 m thickness cover the forearc [*Dingman and Galli*, 1965; *Mortimer and Saric*, 1975] (Figures 1c and 3). These successions were deposited on a subdued, low amplitude pediplain relief. The latter developed during the Eocene to early Oligocene [*Galli*, 1967] by degradation of topographic relief created during Eocene shortening of the Late Cretaceous to Paleogene arc domain (identical to present-day Precordillera). On the basis of apatite fission track data, *Maksaev and Zentilli* [1999] showed that exhumation of the rocks underlying the pediplain occurred rapidly during the Eocene with very little erosion of the Precordillera area since. In the area of what is now the Coastal Cordillera and the Longitudinal Depression, the discontinuity is called the Choja Pediplain [*Galli*, 1967] and has been a coastal plain during the Oligocene as indicated by marine transgressions in southern Peru and northernmost Chile [*Tosdal et al.*, 1984]. Toward the Precordillera area, the Choja pediplain graded into the eroded Paleogene arc, which had a slightly higher elevation (see below) and was only covered by sediments in the late Cenozoic. Most likely it has not only been the sediment source for the Neogene deposits on the western Altiplano flank, but also for the large-scale sedimentary basins found on the Altiplano [*Jordan and Alonso*, 1987; *Horton et al.*, 2001].

3.1. Altos de Pica Formation

[10] At the latitude of 20°30′S the volcano-sedimentary cover is entirely preserved across the plateau flank from the Longitudinal Valley to the western plateau margin (Figure 3). This cover is here termed Altos de Pica Formation (APF) [*Dingman and Galli*, 1965]. The formation comprises continental clastic sediments with intercalated ignimbrites assembled in five subunits: three sedimentary members and two ignimbrite units (Figure 4). The sedimentary units include partly lithified conglomerates and sandstones that were deposited as alluvial detritus along the western Altiplano flank. The basal unit (APF 1) overlies the folded pre-Neogene basement with a major angular unconformity. It consists of fanglomerate, immature sandstone, and polymictic conglomerate with clasts derived from erosion of the underlying basement. The basal fanglomerate thus marks the onset of uplift of the western Altiplano [*Dingman and Galli*, 1965; *Mortimer and Saric*, 1975; *Naranjo and Paskoff*, 1985]. Variation of layer thickness of APF 1 reflects some pre-depositional relief. Average thickness is estimated to be 322 m. The unit thins eastward and pinches out completely at the altitude of 2600 m (Figure 3).

[11] The ignimbrite unit APF 2 conformably overlies APF 1 below 2600 m altitude and disconformably overlies the pre-Neogene basement above this altitude. It covers the entire flank from the plateau to the eastern margin of the Longitudinal Valley where the westernmost outcrops are observed at the longitude of Matilla (Figure 3). Average thickness of APF 2 is 20 m, thickening to the east. Sandstones and conglomerates of APF 3 conformably cover the ignimbrite of member 2. They were deposited in a fluvial regime with some Aeolian intercalations and contain well-rounded basement as well as ignimbrite clasts. Average thickness is estimated to be 200–300 m and can be higher than 500 m. APF 3 thins eastward and pinches out at an altitude of 2300 m. The second ignimbrite unit (APF 4) is up to 150 m thick and conformably overlies the earlier units from the Salar de Coposa in the east down to 2000 m altitude at the toe of the Precordillera to the west. With a minor unconformity, medium to fine grained sandstone and thin conglomeratic beds, that constitute the APF 5, cover the older units from the Longitudinal Valley to the plateau flank where they pinch out at an altitude of 3100 m. The average thickness of APF 5 is 200 m, locally the thickness reaches up to 550 m. Sandstone units in the APF 3 and 5 are increasingly Aeolian in origin and reflect the progressive aridity of the climate described by *Alpers and Brimhall* [1988] and *Gaupp et al.* [1999] for the western Altiplano in northern Chile.

[12] In the well Pintados 1 within the Longitudinal Valley a sequence of the same style as the APF, lacking however the ignimbrite members, unconformably overlies a volcanic basement of Cretaceous age with a basal conglomeratic horizon. This unit is 244 m thick and is overlain by a sequence of lacustrine carbonates as well as evaporates. This latter, so-called Soledad Formation can be correlated to the El Loa Formation of Pliocene to Pleistocene age further south [*Naranjo and Paskoff*, 1985].

[13] Although stratigraphic correlation of clastic sediments is problematic, dated tuff or ignimbrite horizons yield some important constraints (Figure 4). On the Altiplano, internally drained basins contain ignimbrite horizons of APF 4, the Pastillos ignimbrite, and unconsolidated clastic sediments with intercalated rhyolitic tuffs. The Caya Formation conformably covers APF 4 in a 10 km wide and 25 km long basin of the Pampa Caya. It can very probably be correlated chronostratigraphically with member 5 of the APF (Figure 4) and may record the earliest formation of internally drained basins on the plateau margin in the area. A tuff horizon near the top of the unit was dated with 7.0 ± 0.4 Ma [*Baker*, 1977]. The age of the Coposa Formation that unconformably overlies APF 4 in the Salar de Coposa depression was determined with 5.34 ± 0.2 Ma at the base [*Vergara and Thomas*, 1984] and 3.6 ± 0.3 Ma at the top [*Baker*, 1977] and is hence younger than the Caya Formation. The youngest ignimbrite in this area, the Pastillos

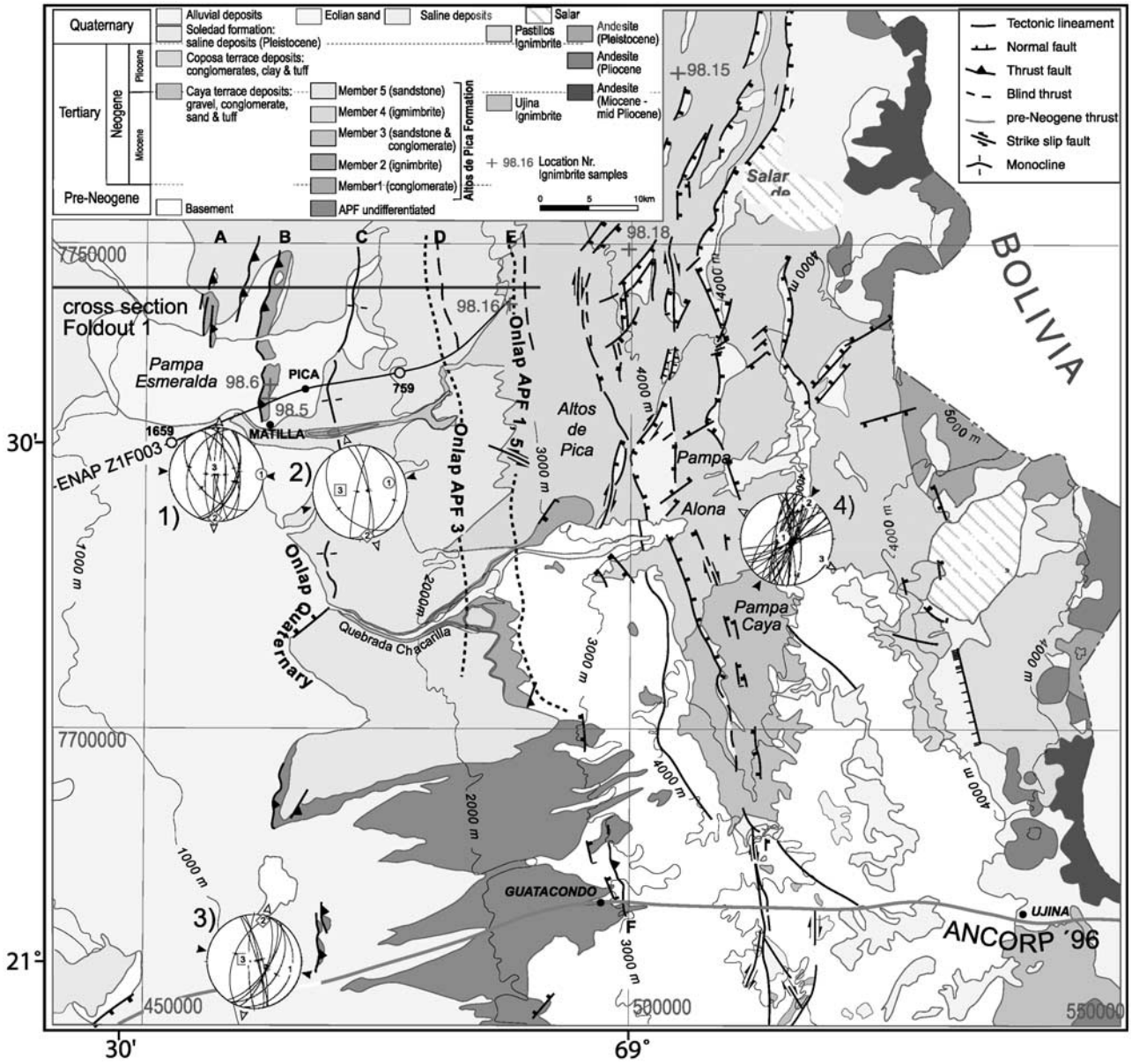

Figure 3. Geological map of the study area showing distribution of Neogene to Quaternary magmatic and sedimentary deposits as well as tectonic structures. N–S trending thrust faults and monoclinal flexures dominate at the base and flank of the western monocline. Kinematic analysis in deformed Neogene deposits depicted in stereograms 1–3 indicates W–E directed shortening. The plateau margin itself is segmented in numerous internally drained basins by normal and strike-slip faults. Stereogram 4, showing results from kinematic analysis of these faults, indicates NW–SE directed extension with dextral strike-slip motion along N–S trending faults that represent the northern parts of the Precordilleran fault system. Older NNW–SSE trending thrust faults are exposed in the pre-Neogene basement.

ignimbrite, overlies the Coposa Formation and was dated by *Baker* [1977] at 0.73 ± 0.16 Ma.

[14] South of the Quebrada Chacarilla, the APF deposits are less well differentiated due to a lack of intercalated volcanics. On the plateau margin toward the south, the so-called Sichal Formation, coarse clastic sediments of Oligocene to early Miocene age [*Maksaev*, 1978], may encompass the entire range of APF deposition: the up to 900 m thick unit is conformably covered by the Ujina Ignimbrite with an age of 9.3 ± 0.4 Ma.

3.2. APF Ignimbrites: Sr, Nd Isotope Systematics and Age Constraints

[15] In spite of a larger number of published K-Ar ages on biotite and whole rock ages of the ignimbrites [*Baker*,

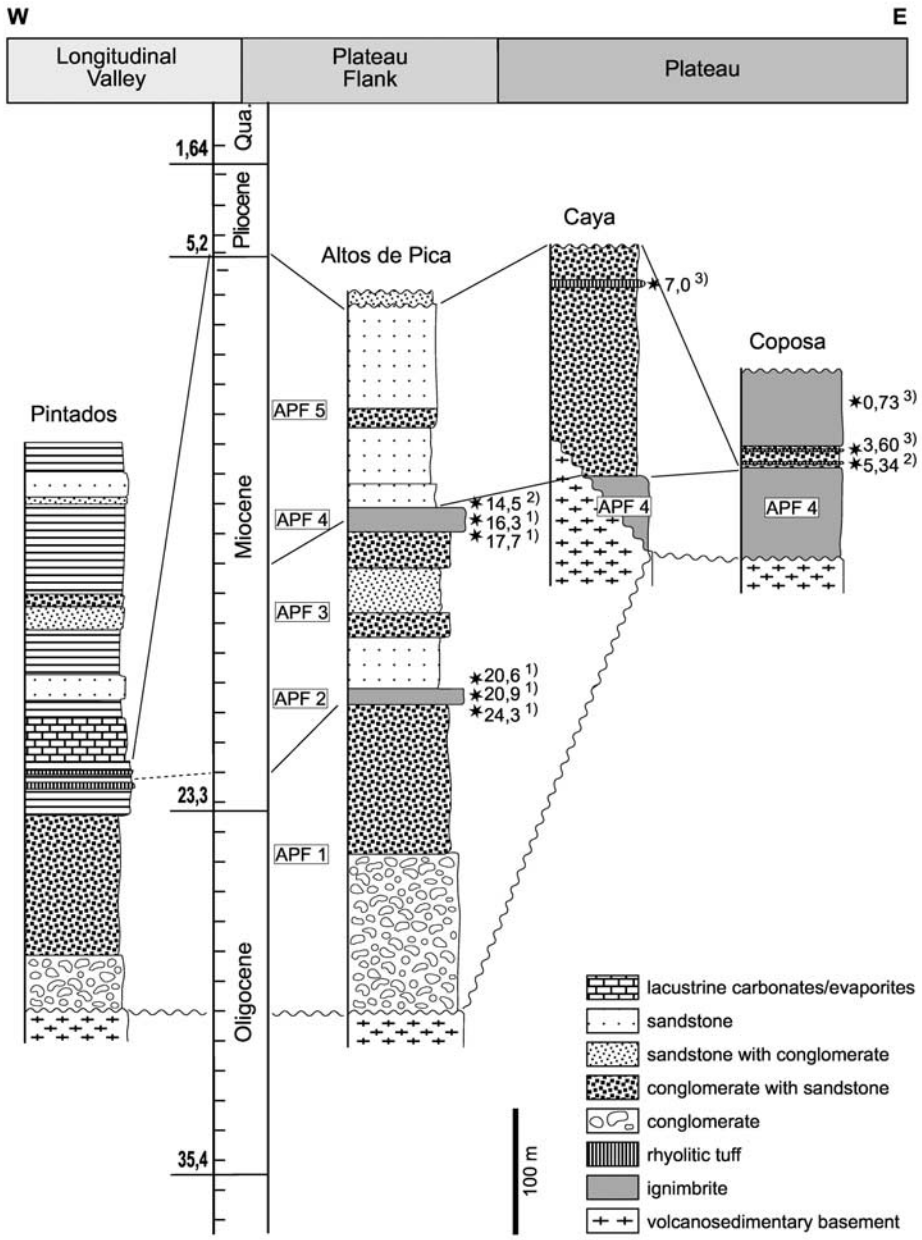

Figure 4. Stratigraphic columns of Oligocene to Quaternary volcano-sedimentary deposits between 20° and 21°S. Columns are scaled to vertical thickness. Correlation is based on stratigraphic horizons with well established ages (sources labeled as follows: 1, this paper; 2, *Vergara and Thomas* [1984]; 3, *Baker* [1977]). Correlation with stratigraphic section in the Longitudinal Valley (well Pintados I, courtesy of ENAP) are based on lithostratigraphic observations.

1977; *Baker and Francis*, 1978; *Vergara and Thomas*, 1984; *Naranjo and Paskoff*, 1985; *Vergara et al.*, 1986] age resolution of the APF is not well constrained. This is mainly due to unconstrained sampling in the sequence without differentiation of the various ignimbrite members and identification of their precise stratigraphic location within the sequence. Therefore we took samples of ignimbritic rocks for this study at the lowermost and topmost positions within the two ignimbrite members with the aim to resolve the internal chronology of the APF, and to provide time constraints on its deformation. The ignimbrites have rhyolithic bulk chemistry, with 73–76% SiO_2. They carry 20–40 vol % of phenocrysts in glassy matrix. Phenocrysts are quartz, feldspar, (oxy)biotite, hornblende as well as trace amounts of apatite, zircon, monazite, pyroxene (pigeonite) and magnetite. They can be termed as large-volume ignimbrites; a conservative volume estimate of all APF ignimbrites is >240 km^3 [*de Silva*, 1989].

Table 1. Age Data for the Altos de Pica Formation

Number	Location	Unit	Method	Age	Author
1	~20°09/69°19	undefined	K-Ar whole rock	17.3 ± 0.5	*Vergara et al.* [1986]
2	~20°09/69°19	undefined	K-Ar whole rock	18.6 ± 0.3	*Vergara et al.* [1986]
3	~20°12/69°21	undefined	K-Ar whole rock	17.4 ± 0.1	*Vergara et al.* [1986]
4	20°39 40/68°43 17	undefined	K-Ar biotite	14.7 ± 0.4	*Vergara and Thomas* [1984]
5	20°26 10/68°52 30	undefined	K-Ar biotite	14.6 ± 0.4	*Vergara and Thomas* [1984]
6	20°15 20/68°52 30	undefined	K-Ar biotite	14.5 ± 0.4	*Vergara and Thomas* [1984]
7	20°14 00/68°52 45	undefined	K-Ar biotite	15.5 ± 0.8	*Baker* [1977]
8	20°42 15/68°55 45	undefined	K-Ar biotite	17.1 ± 0.8	*Baker* [1977]
9	20°30 00/68°55 40	undefined	K-Ar biotite	14.6 ± 0.3	*Baker* [1977]
10	20°32/69°20	undefined	K-Ar biotite	16.2 ± 0.4	*Baker* [1977]
11	19°53 55/68°40 30	undefined	K-Ar biotite	16.5 ± 0.6	*Baker and Francis* [1978]
12	20°03/69°03	undefined	K-Ar biotite	18.2 ± 0.9	*Naranjo and Paskoff* [1985]
13	20°04/69°07	undefined	K-Ar biotite	22.6 ± 1.6	*Naranjo and Paskoff* [1985]
A98.6	20°29.380′S/69°21.280′W	APF 2	Bi – hbl isochrones	24.33 ± 0.26	this work
A98.5	20°29.109′S/69°21.304′W	APF 2	Bi – hbl isochrones	20.90 ± 0.21	this work
A98.18	20°18.967′S/69°00.815′W	APF 2	Bi – hbl isochrones	20.61 ± 0.21	this work
A98.16	69°06.793′S/20°24.130′W	APF 4	Bi – hbl isochrones	17.67 ± 0.18	this work
A98.15	20°12.862′S/68°59.210′W	APF 4	Bi – hbl isochrones	16.27 ± 0.16	this work

[16] For Rb-Sr and Sm-Nd isotope analyses, five ignimbrite samples were processed (see Figure 3 for sample locations). Whole rock powders as well as mineral separates of feldspar, biotite and hornblende were produced. Biotite was ground under ethanol in a polished agate mortar and then sieved in ethanole to obtain clean, inclusion-free separates. Mineral concentrates were finally purified by hand-picking under the binocular microscope. However, some feldspar crystals were intimately intergrown with the glassy matrix so that feldspar separates may have carried some glass (<5%). Samples were processed following standard dissolution and cation exchange techniques, and analyzed by isotope dilution for Rb, Sr, contents. Sm and Nd contents were determined by ICP-AES. Determinations of Sr, Rb isotope ratios were carried out on a VG Sector 54 multicollector TIMS, of Nd isotope ratios on a Finnigan MAT 262 mass spectrometer, both at the GFZ Potsdam. Total blank values were consistently very low (<0.15 ng for all elements), and no blank correction was applied. Data reduction and age calculations were carried out using the program Isoplot/Ex [*Ludwig*, 1999]. Age uncertainties are given at the 2 sigma level. In the calculation of isochron ages and initial isotopic compositions, standard errors of ±1% for $^{87}Rb/^{86}Sr$, ±0.003% for $^{87}Sr/^{86}Sr$, ±5% for $^{147}Sm/^{144}Nd$, and ±0.002% for $^{143}Nd/^{144}Nd$ ratios were applied if individual errors were smaller than these values.

3.3. Results

[17] Results of the Rb/Sr and Sm/Nd isotope analyses are presented in Tables 1, 2, and 3. For some samples, the Rb/Sr mineral and whole rock data did not yield perfect isochrons. Detailed investigation of the samples reveals that this can be attributed to local devitrification of the glassy matrix. Biotite and hornblende were not affected by alteration. Consequently, extrusion ages of the ignimbrites were calculated using hornblende-biotite mineral pairs. For all samples, the ages calculated that way match, within limits of error, ages derived from biotite-feldspar pairs. Since hornblende is a low Rb/Sr phase, precise initial $^{87}Sr/^{86}Sr$ values for the ignimbrite magmas are obtained, in the range between 0.7056 and 0.7059. As to the Nd isotopic composition, $\varepsilon_{Nd}(t)$ is between −3.4 and −3.8. Both the Sm/Nd and Rb/Sr data sets reveal regular, apparently undisturbed, quasilinear trends for the isotopic evolution in the magma source region. Figure 5 shows the correlations between initial Sr and Nd isotopic compositions, and extrusion ages of the ignimbrites.

[18] The extrusion ages for the APF ignimbrites span a range from 24.33 ± 0.26 Ma to 16.27 ± 0.16 Ma. APF member 2 was extruded between 24.33 ± 0.26 Ma and 20.61 ± 0.21 Ma. Since sampling of the APF member 4 only comprised the deeper parts, the unit 4 eruption interval is likely to have continued from 17.67 ± 0.18 Ma (this work) to 14.5 ± 0.4 Ma (youngest K-Ar biotite age) [*Vergara and Thomas*, 1984]. All other age information published for APF ignimbrites [*Baker*, 1977; *Baker and Francis*, 1978; *Vergara and Thomas*, 1984; *Naranjo and Paskoff*, 1985; *Vergara et al.*, 1986] falls in the range between circa 23 and circa 14.5 Ma.

[19] Using the age difference between members 2 and 4 to calculate sedimentation rates, a first order estimate of the age of the base of the APF is attempted, based on the average thickness of member 1. An average sedimentation rate of 0.008 cm/yr calculated for APF 3 yields an estimate of ~27–29 Ma for the base of the APF. This value correlates with the reported age of ~29 Ma of the widespread unconformity at the base of the "Gravas de Atacama" that overlies the same type of basement further south [*Haschke and Günther*, 2003]. The entire age data set from the APF and the overlying formations therefore embraces the time from the middle Oligocene to the late Pleistocene, i.e., the time of uplift of the Altiplano plateau (Figure 3).

4. Deformation of the Plateau Flank

4.1. Structural Mapping

[20] At the surface of the plateau flank, structures reflecting deformation include gentle folds and minor faults.

Table 2. Rb/Sr Analytical Data for Ignimbrites, Altos de Pica Formation[a]

Sample, Analysis No.	Material	Rb, ppm	Sr, ppm	$^{87}Rb/^{86}Sr$	$^{87}Sr/^{86}Sr \pm 2\sigma_m$
98-5 (Age: 20.90 ± 0.21 Ma; $^{87}Sr/^{86}Sr$ Initial: 0.70573 ± 0.00004)					
PS44	biotite	289.2	9.27	90.47	0.732587 ± 0.000010
PS51n	feldspar	102.2	33.32	8.870	0.708439 ± 0.000013
PS82	whole rock	148.1	32.67	13.12	0.709611 ± 0.000011
PS81	hornblende	5.010	128.5	0.113	0.705763 ± 0.000038
98-6 (Age: 24.33 ± 0.26 Ma; $^{87}Sr/^{86}Sr$ Initial: 0.70564 ± 0.00002)					
PS41	biotite	264.4	35.59	21.51	0.713074 ± 0.000011
PS47	feldspar	85.42	56.02	4.411	0.707239 ± 0.000010
PS85	whole rock	111.4	64.33	5.009	0.707743 ± 0.000009
PS73	hornblende	16.08	92.00	0.506	0.705816 ± 0.000011
98-15 (Age: 16.27 ± 0.16 Ma; $^{87}Sr/^{86}Sr$ Initial: 0.70589 ± 0.00002)					
PS45	biotite	381.9	11.45	96.66	0.728229 ± 0.000015
PS49	feldspar	163.4	120.4	3.928	0.706703 ± 0.000010
PS71	whole rock	194.4	124.2	4.529	0.706839 ± 0.000010
PS77	hornblende	15.62	225.7	0.200	0.705935 ± 0.000011
98-16 (Age: 17.67 ± 0.18 Ma; $^{87}Sr/^{86}Sr$ Initial: 0.70584 ± 0.00002)					
PS43	biotite	357.6	23.37	44.32	0.716962 ± 0.000013
PS48	feldspar	167.4	104.9	4.618	0.706882 ± 0.000010
PS69	whole rock	179.5	136.6	3.802	0.706745 ± 0.000034
PS78	hornblende	10.00	238.0	0.122	0.705871 ± 0.000011
98-18 (Age: 20.61 ± 0.21 Ma; $^{87}Sr/^{86}Sr$ Initial: 0.70580 ± 0.00002)					
PS42	biotite	300.9	16.57	52.63	0.721202 ± 0.000011
PS50	feldspar	110.7	29.23	10.96	0.708996 ± 0.000011
PS84	whole rock	136.9	44.22	8.957	0.708681 ± 0.000011
PS72	hornblende	12.80	188.0	0.197	0.705856 ± 0.000017

[a]An error interval of ±1% has to be assigned to the Rb/Sr ratios. Isochron parameters are calculated for biotite-hornblende pairs (see text for discussion).

Reverse faults are exposed in deeply incised bedrock channels draining the plateau flank toward the west. In the Longitudinal Valley and at the base of the flank, faults are obvious from N–S striking ridges exposing pre-Neogene basement, upper Oligocene to lower Miocene sediments and lower Miocene ignimbrites (APF 2) in the hanging wall (i.e., faults A, B and E, Figure 3). These ridges are typically formed from open folds with a longer, east dipping backlimb and a shorter, west dipping forelimb that is not always present (Figures 6a and 6b). In outcrops, small-scale reverse faults are exposed at their forelimbs and show vertical offsets in the order of centimeter to decimeter scale (Figure 6c). Weak striations on the fault surfaces or the gouge are consistently downdip. Near the regional surface, these structures are usually onlapped or covered by late Miocene to Quaternary deposits (Figures 6a and 6b). Because of this structural style, the plateau flank exhibits a stepped morphology with broader, shallow west or east dipping segments (0°–3°) and steeper, west dipping monoclinic flanks (6°–12°; see Figure 2). Both exhibit a common wavelength of several kilometers. Channels crossing the monoclinic flanks higher up on the plateau flank expose N–S striking reverse faults that dip steeply to the east with a spacing of several 10–100 m and displacements at the same order of magnitude (Figure 6e). Large- as well as smaller-scale reverse faults predominantly strike N–S and dip 40°–70° to the east with some conjugate west dipping faults. Paleostress analysis on these faults using the P/T method

Table 3. Sm/Nd Analytical Data for Ignimbrites, Altos de Pica Formation[a]

Sample, Analysis No.	Sm, ppm	Nd, ppm	$^{147}Sm/^{144}Nd$	$^{143}Nd/^{144}Nd \pm 2\sigma_m$	ε_{CHUR} (t)
98-5 wr (PS139)	3.2	18	0.108	0.512435 ± 0.000008	−3.7
98-6 wr (PS138)	3.5	22	0.097	0.512427 ± 0.000007	−3.8
98-15 wr (PS135)	4.0	22	0.110	0.512451 ± 0.000008	−3.4
98-16 wr (PS137)	4.1	22	0.113	0.512448 ± 0.000009	−3.5
98-18 wr (PS136)	3.4	19	0.108	0.512431 ± 0.000007	−3.8

[a]Sm and Nd abundances were determined by ICP-AES at the GeoForschungsZentrum Potsdam. An error interval of ±5% has to be assigned to the Sm/Nd ratios. Here ε_{CHUR} (t) is calculated for the extrusion ages given in Table 2. For sample details see Table 2.

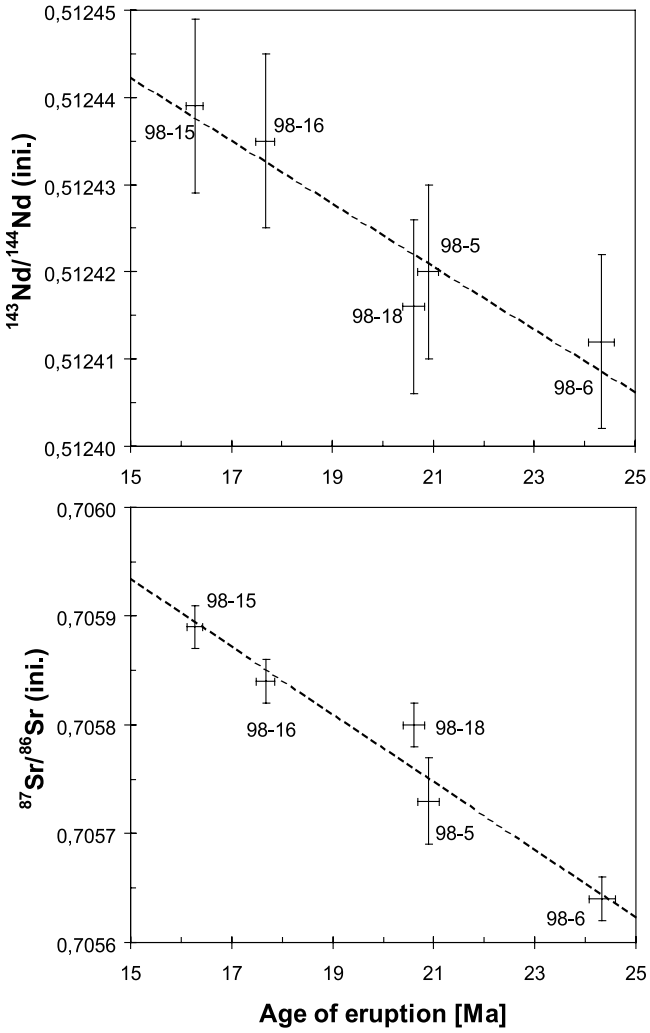

Figure 5. Correlations between ages of ignimbrite eruption and initial $^{87}Sr/^{86}Sr$ and initial $^{143}Nd/^{144}Nd$ ratios. Quasilinear trends indicate undisturbed isotopic evolution of the magma source region.

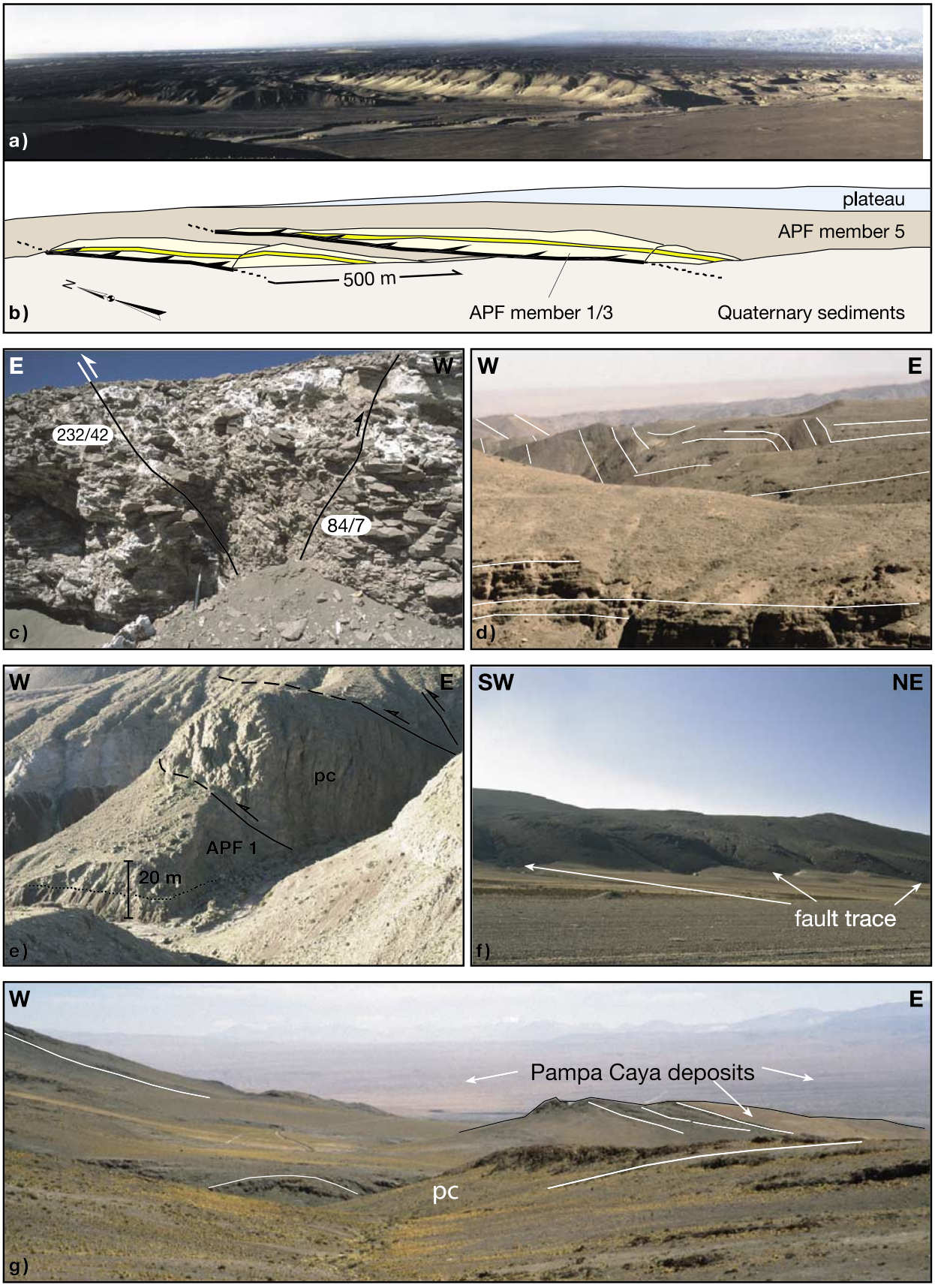
a)
plateau
APF member 5
500 m
b)
APF member 1/3
Quaternary sediments
E
W
232/42
84/7
c)
W
E
d)
W
E
pc
APF 1
20 m
e)
SW
NE
fault trace
f)
W
E
Pampa Caya deposits
pc
g)

Figure 6

[*Turner*, 1955] yields an average E-W directed compression (see Figure 3).

[21] As a general trend, reverse faults and folds are more prominent and better exposed near the toe of the plateau where they consistently affect all exposed APF units (Figure 3). Toward the higher parts of the plateau flank, the number of exposed reverse faults decreases substantially and the amplitude of associated geomorphic features decreases. Exposed structures in bedrock channels are often completely covered by younger deposits forming the present surface or were downgraded by erosion. The highest observed reverse faults (at ~3000 m altitude, Figures 2 and 3) affect only pre-Neogene basement and lower Miocene sediments (APF 1; Figures 3 and 6e) and show tabular hanging wall geometry as opposed to the hanging wall folds at the west flank toe. Younger APF members cover these reverse faults without being affected. On the plateau margin, reverse faults are only exposed in the pre-Neogene basement units that were deformed during the Eocene [*Scheuber and Reutter*, 1992; *Scheuber et al.*, 1994]. In the same area, the Pampa Caya deposits onlap the hanging wall backlimb east of fault F (Figure 6g), which here only exposes basement rocks, in a low-amplitude, long-wavelength depression. The parallel attitude of Paleogene structures and the here-reported Neogene structures suggest that the older structures may have controlled the architecture of the Neogene faults.

[22] Virtually all geologic units are affected by an extensional and strike-slip fault system, forming well-defined escarpments (Figure 6f). These faults strike N–S to NE–SW and are concentrated especially along the plateau margin where they are responsible for the formation of internally drained basins (Figures 2 and 3). Normal faults with the same orientation can be observed also in the Longitudinal Valley, on the plateau flank, and in the Western Cordillera where they even offset the youngest Quaternary units. A major strike-slip system, exposed in the Precordillera, parallels the plateau margin and is identified as the northward continuation of the Precordilleran Fault System. In the northeastern part of the working area, a major releasing bend in this system is responsible for the formation of pull-apart basins including the Pampa Caya, Pampa Alona and the Salar de Huasco (Figure 3). A dextral sense of slip is derived from offset streams and shutter ridges (Figure 6f) for all strike-slip faults trending N–S to NNW–SSE. Kinematic analysis of both strike-slip and normal faults on the plateau margin yields a consistent kinematic system of oblique NW-SE directed extension (Figure 3).

4.2. Reflection Seismic Data

[23] Two reflection seismic lines cross all or part of the analyzed area: (1) the ANCORP'96 line, a low-fold dynamite near-vertical-incidence reflection seismic line that traverses the entire plateau flank, but only images structures deeper than some 10 km [*ANCORP Working Group*, 1999, 2003], and (2) the industry reflection seismic line Z1F003 provided by ENAP (Empresa Nacional del Petroleo, Chile). The latter was available as a coherency-filtered stack section that traverses the entire Longitudinal Valley to about 3000 m altitude on the plateau flank (see Figures 1a and 3 for line locations).

[24] The reflection section Z1F003 and the line drawing (Foldout 1) show an excellent match with the structures observed in the field: equidistant upright open folds associated with thrusts link with the mapped fault related folds or major monoclines (e.g., shot points 1269, 1049, 250). In several instances, the seismic record also exhibits basement steps, which do not show up in geomorphic features (i.e., group of faults labeled D in Foldout 1; see also Figure 6d). APF members 3 and 4 or higher parts of APF 5 cover these at this position. All imaged structures show intervening piggyback basins that were not obvious from surface observations. The reflector geometries exhibit well-defined onlap patterns or wedge-shaped depositional units at the flanks of these antiforms. According to these and the equivalent field observations, we interpret these structures as growth structures that developed as fault-bend folds in the hanging wall of reverse faults or as drape folds in the sediments overlying the basement thrust faults (Foldout 1c).

[25] The top of the pre-Neogene basement is obvious from downward loss of layered reflectivity. This depth also correlates with the drilled basement depth at the Pintados 1 well further west in the Longitudinal Valley (i.e., 580 m below surface at 1000 m elevation) and with the basement-cover interface projected from the surface. The averaged interval velocities allow calculating the elevation of the top of the basement at some 200 m below sea level near the deformation front (shot point 1659; Foldout 1c). While surface exposure and the seismic line both exhibit some local variability of the depth to basement—i.e., some pre-Neogene very long wavelength relief with an amplitude of less than a few 100 m—the above numbers underscore the

Figure 6. (a) View of toe of plateau flank (toward NE) displaying fault bend folds that expose stratified sediments of the lower Altos de Pica Formation dipping with 15° toward 90°E in two N–S trending ridges. Ridges are unconformably onlapped by mildly tilted APF member 5 and undeformed? Quaternary alluvial deposits (SW part of study area). (b) Interpretation of Figure 6a. (c) Minor reverse faults with dip-slip lineations crosscutting west dipping ignimbrites of APF member 2 at fault B near Matilla (see map). (d) Northward view of upper plateau flank (north of Guatacondo) showing gently inclined to strongly folded Altos de Pica Formation at ~3000 m altitude (structures related to fault E). (e) Cretaceous sediments (pc) thrust on top of APF member 1 along several reverse faults (parts of fault F north of Guatacondo) dipping between 40° and 70°E. (f) Marginal fault of Salar de Huasco basin showing a minimum of 100 m vertical displacement. Shutter ridges indicate a dextral component of strike-slip motion. (g) Northward view over Pampa Caya showing mildly folded to gently westward inclined Cretaceous and Paleogene rocks unconformably onlapped by east dipping Pampa Caya deposits.

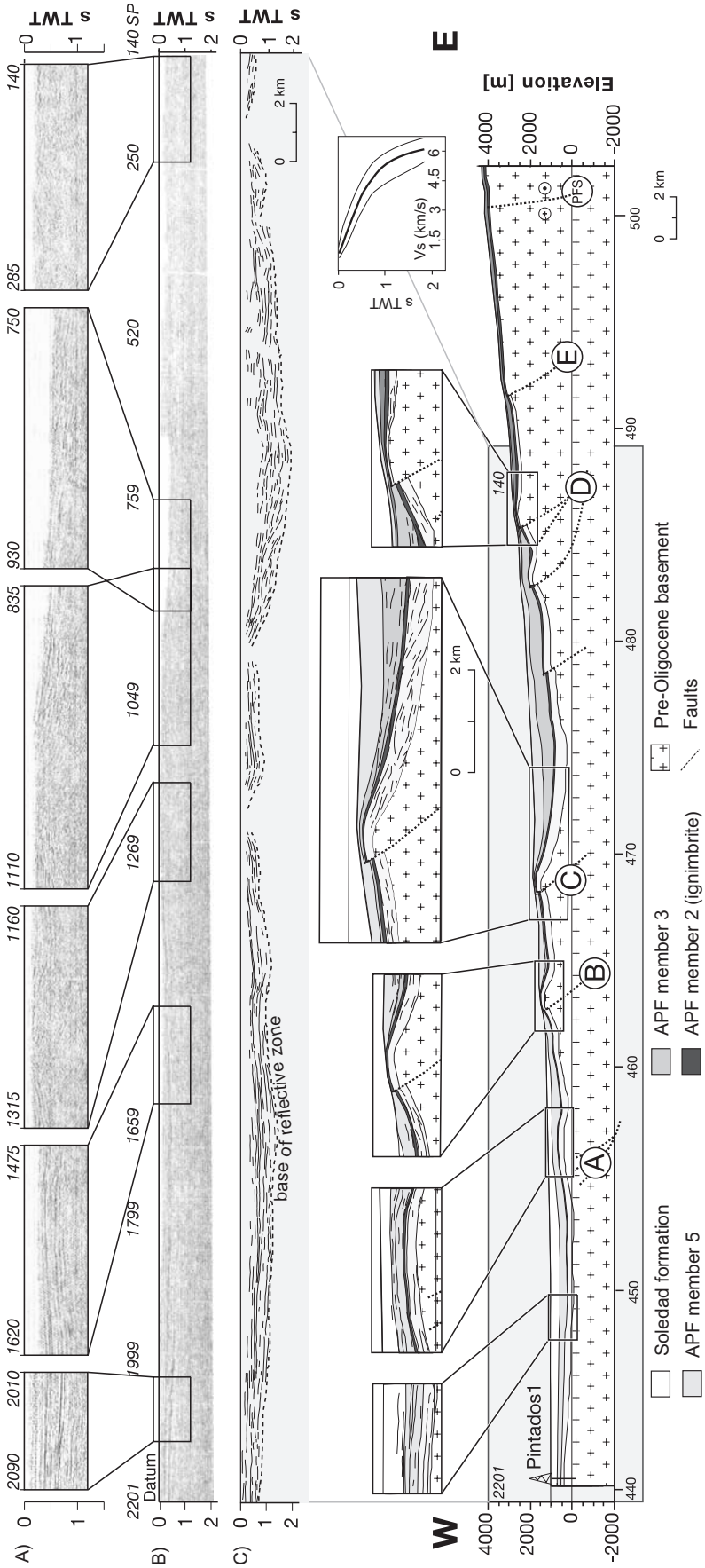

Foldout 1. (a) Reflection seismic line Z1F003 (courtesy of ENAP) as a coherency filtered stack section with enlargements showing local detail; see Figures 1 and 3 for location of line. (b) Line drawing of reflection section in Foldout 1a. Datum is local elevation. (c) Interpreted section using surface data and well Pintados 1 after projection of line drawing in EW section (see Figure 3 for location) and depth conversion based on interval velocities (see inset); enlargements largely identical with Foldout 1a. Letters A to E refer to faults in Figure 3. PFS, westernmost branch of Precordilleran fault system. See enlarged version of this figure in the HTML.

general trend of deepening of the basement below the Longitudinal Valley toward the plateau flank in the east (Foldout 1c). Using the same interval velocities, we identified the amplitudes of the folds or the offset at faults at typically a few 100 m increasing eastward to a maximum of some 800 m.

4.3. Drainage Basin Analysis

[26] Analyses of drainage patterns and stream profiles [*Merritts and Vincent*, 1989; *Keller and Pinter*, 2002] are used to extend the above observations from field mapping and seismic imaging to the higher parts of the plateau flank and along strike (Figure 7). From the absence of major lithological contrasts in the Neogene cover, we expect the observed pattern to image tectonic structures. The presently dry streams cut across most Neogene units, in the south down to the basement, and drain the plateau flank in an E–W direction. Uplift of the western plateau has formed the present drainage divide, defeating all upper plateau-draining channels but one. The divide isolates a series of NS trending basins on the plateau that are internally drained or linked to longitudinal drainage into the Rio Loa system in the southeast (Figure 7).

[27] The analysis of stream gradients of 18 streams shows up to three well-defined nick points in the individual stream profiles. The stream profiles next to the well exposed geology at Pica and the parallel reflection seismic section show an excellent correlation of the position of nick points with the fronts of monoclines, folds, and faults above the present deposition-erosion limit (Foldout 1c and Figure 8). This also includes cases where faults and associated folds are entirely covered by younger deposits between shot points 550 and 200. Correlation of nick points in the stream profiles can be traced along strike of the plateau flank at similar elevations and can be shown to link with other faults exposed in deeper incised channels. Nick points also trace the onlaps of APF 1 and APF 3. This strategy helped to map three additional faults on the upper plateau flank (faults D, E, F) where geomorphic steps are absent or less conspicuous. Toward the north, the easternmost fault F probably dies out or follows the drainage divide. The fault traces as identified from this analysis have lengths in the order of 25–55 km. As shown from the length of the morphological steps and from the exposed and inferred faults in Figures 3 and 7, the individual fault systems probably consist of linearly arranged structures rather than of a single coherent fault.

4.4. Results

[28] Using surface observations, stratigraphic framework, well data, reflector geometries, and drainage basin analysis, an interpreted geological section (Foldout 1c) provides a kinematic sequence of the structural evolution. The age of the two easternmost faults (labeled E and F, Figures 3 and 8) that are only exposed in the more deeply exhumed area south of Quebrada Chacarilla is indirectly constrained from two observations. (1) Fault E forms the eastern onlap limit of initiation of sedimentation in the Oligocene (~27–29 Ma; APF member 1) on the largely eroded and subdued pre-Neogene basement surface (seen best at flanks of the Quebrada Chacarilla); Fault F limits APF sedimentation south of the same Quebrada (due to lacking younger cover in the latter case, this may also be overprinted by later erosion). Probably, topography resulting from activation of these faults triggered hanging wall erosion and westward redeposition by creating the first relevant relief on the post-Eocene peneplain in the Precordillera area. (2) Motion on fault E was terminated by the time of eruption of the APF 2 ignimbrite member. Only the minimum displacement of both faults is constrained as the hanging wall basement may have been eroded substantially as indicated by the APF 1 member thickness in the footwall. Later reactivation of these faults during or after deposition of the APF 4 ignimbrite member is indicated again by two aspects: (1) Fault E precisely delimits the eastern onlap of APF member 5 (corresponding to onlap of member 1), and (2) both faults (E and F) formed accommodation space for ignimbrites and the Late Miocene Caya Formation in the Pampa Caya (Figure 6g). These observations constrain two phases of activity for faults E and F, the first between circa 30 up to 24 Ma and the second between some 16 and 7 Ma.

[29] Fault D—a composite system of several probably linked faults—confines the eastern onlap of APF member 3 and forms the western limit to ignimbrite outflow of APF member 4. The relief due to fault activation may have been responsible for both effects. Seismic interpretation and surface data indicate that APF member 1 and 2 were folded by this fault system—along with some erosion—and that member 5 covers this fault undeformed. Activation of fault D therefore is mainly constrained to the time span between 24 and 15 Ma.

[30] Fault C affected APF members 1 and 2 by folding and minor erosion; the folded member 3 shows wedge-shaped thinning and tilting on both limbs, but its upper parts partly cover the blind fault. APF member 5 shows thinning, but no obvious tilting. The period of fault activity is accordingly bracketed between 20 and <14 Ma. At fault B, APF member 3 pinches out before reaching present surface. The older members and the partly exposed basement ridge are deformed and eroded at the hinge, and member 5 is most strongly affected forming growth structures on both flanks up to the youngest exposed beds at surface. Activity occurred therefore most probably between <17 and <10 Ma. Fault A is well exposed NW of Pica, while it dies out toward the south and shows only minor buckling at the site of the seismic line. It deforms APF members 1 and 2. Member 3 does not appear to be existent, or may be represented by a sand unit (25 m thick) in the base of member 5 as found in well Pintados 1. In the reflection as well as in surface data, only bedding of the higher parts of member 5 shows progressive onlap and decreasing tilting upsection. The age span for activation of fault A would accordingly be between <14 and <10 Ma, but no later than the end of Miocene. The Plio-Pleistocene Soledad Formation and younger alluvial deposits onlap both structures, A and B, without tilting.

[31] Apart from the end of deposition of APF member 5 and the Caya Formation, the end of compressive deforma-

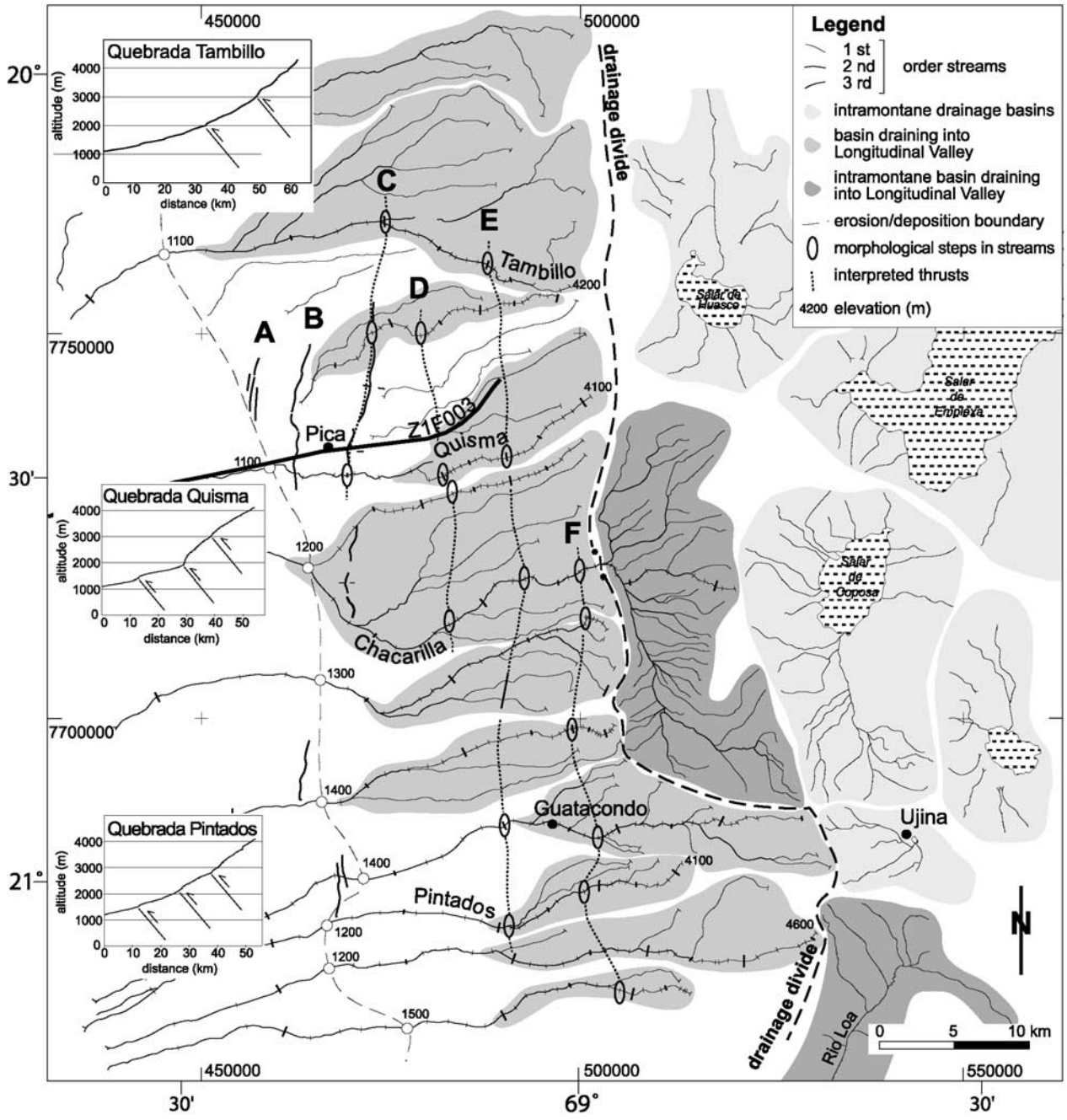

Figure 7. Drainage basin morphology of the study area showing intramontane basins on the plateau and streams draining the western flank toward the Longitudinal Valley where they are abandoned. Longitudinal profiles of selected streams show steep gradients continuing to the mouth in the Longitudinal Valley. Nick points in stream profiles can be correlated with thrust faults or west facing monoclines. In map view, these steps are marked with an oval. The stippled lines connecting morphological steps correlate well with mapped thrust faults and are interpreted as the trend of thrust faults or growth folds along the plateau flank.

tion in this area is constrained by the onset of transtensional deformation forming internally drained pull-apart basins. Deposition of the Coposa Formation probably marks the first sediments deposited in a purely extensional basin indicating that extensional deformation started at least 5.3 Ma ago (age of oldest tuff in Salar de Coposa basin [*Vergara and Thomas*, 1984]). This is in good agreement with the age of 4.8 Ma given by *Muñoz and Charrier* [1996] for the definite end of contractional deformation along the west vergent thrust system between 18°–19°S.

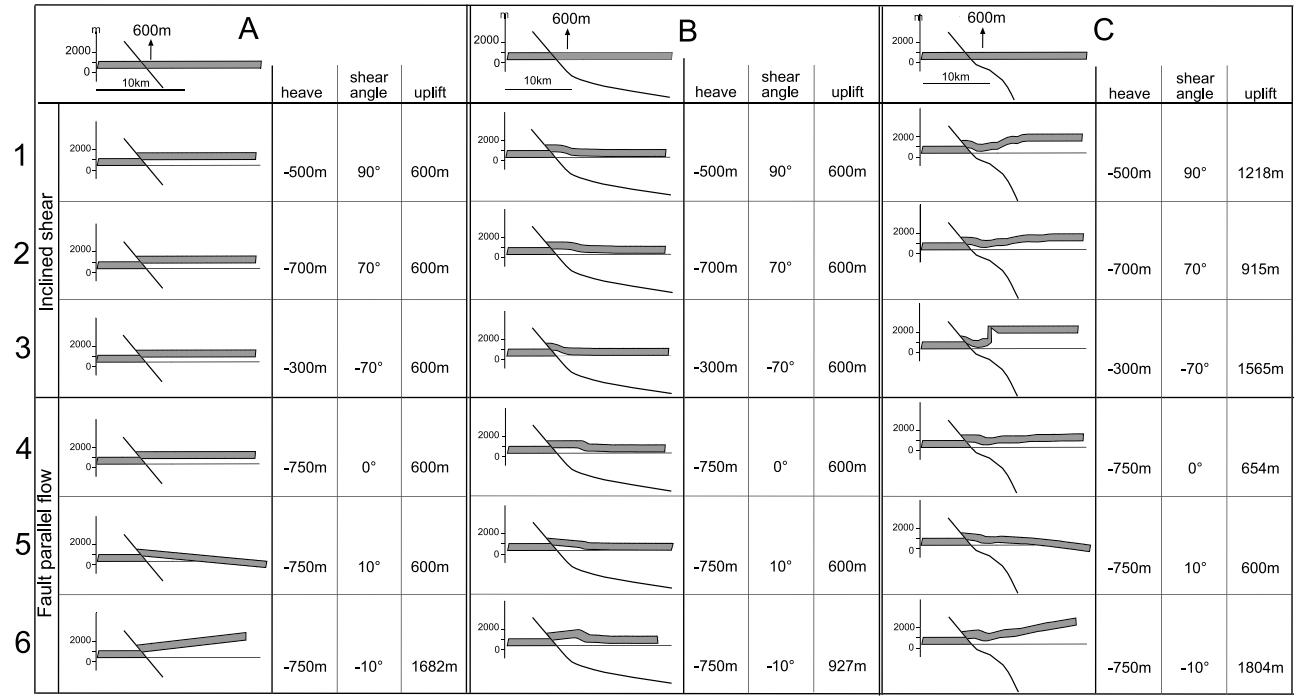

Figure 8. Sensitivity analysis showing dependence of hanging wall deformation on fault geometry, shear mode, and shear angle at constant uplift for a fault (a) with constant dip, (b) with ramp-flat trajectory, and (c) with ramp-flat-ramp trajectory.

[32] In summary, the kinematic observations indicate that a west vergent belt of reverse faults of 50 km width underlies the western flank of the Altiplano plateau. This fault system shows progressive westward younging and formed during a period of E–W contraction that started at ~30 Ma and terminated between 7 and 5.3 Ma. Final motions at the front of this fault system were synchronous to out-of-sequence reactivation of the more internal faults with a retreat of onlap limits to higher altitudes. This deformation stage is followed at around 5.3 Ma by a still active NW–SE transtensional stage that reactivated the Precordilleran fault system in dextral mode. This stage mainly affected the plateau margin, but, locally, also extended to the plateau flank and the Longitudinal Valley.

5. Deformation Modeling

[33] Where deformation is weak and structural information from the surface and seismic data lacks precision, structural constraints may be insufficient to assess the deep continuation of near surface structures. We therefore employ a modified approach with respect to standard section construction and validation techniques by systematically mapping the solution space defined by the variables related to hanging wall deformation. This warrants a more complete analysis of structures at depth including an assessment of the robustness of the solution with respect to constraining data. The software-based technique, using 2D-MOVE® (Midland Valley Corporation, Glasgow, UK), involves (1) an initial sensitivity analysis of structural geometries with respect to restoration algorithms and variation of their parameters aiming at identifying the most promising algorithm and parameter combination, and (2) an iterative restoration of the entire structural association using the above analysis and based, additionally, on a set of fundamental constraints derived from field observations and seismic data.

5.1. Sensitivity Analysis

[34] The sensitivity analysis was performed using the inclined-shear method [*Rowan and Kligfield*, 1989] and the fault-parallel flow method [*White et al.*, 1986]. These two mechanisms best reflect the structures observed at the Altiplano flank, which are dominated by faulting and slip on shear planes crosscutting both the unconsolidated APF series at high angles to bedding as well as the fractured basement. In both approaches, the relevant variables are fault geometry, fault displacement, and shear angle. The starting models included three fundamentally differing fault geometries with an averaged near-surface fault dip of 50° and a vertical uplift at the fault of 600 m. The best fit solution was defined by its ability to reproduce the observed structures. The key features to be reproduced were (1) the various styles of hanging wall deformation (open folds with thrust-top basins versus tabular hanging walls), (2) the regional tilting of the surface of the entire structure. Hanging wall growth folds are only produced by (1) a fault with a ramp-flat trajectory or (2) with a ramp-flat-ramp trajectory (Figures 8b and 8c). Tabular uplift and tilting of the hanging wall only occurs at faults with rather constant dip (Figure 8a). Regional tilting and uplift of the hinterland in conjunction with a frontal fold is only

produced by a fault with ramp-flat-ramp trajectory. This uplifting hinterland part constrains a thrust top basin between the frontal fold and the hinterland, as observed in the seismic data. Single planar, deep-reaching faults (Figure 8a) are definitely excluded for their inability to generate the geometry of the entire west flank.

[35] Further analysis helped to reject fault-parallel flow as a deformation mechanism for several reasons: fold geometry is less well reproduced; very minor deviations from perfect fault-parallel shear produced substantial regional tilting even at minor displacement. This effect is not observed in the frontal, i.e., less displaced, thrust units of the here-analyzed system. In addition, exposed secondary faults and shear planes indicate a conjugate pair of faults around a subvertical bisector, which rather lends support to the assumption of an inclined shear mechanism with steep shear plane. Last, but not least, the ramp-flat-ramp geometry of a basal master fault yields the best first-order image of the monoclinic flank geometry as observed for the entire plateau margin. In summary, at a given deformation mode, the fault geometry exerts a stronger control on the modeling result than the shear angle.

5.2. Restoration Procedure

[36] The individual structures were restored with the following strategy. Every structure was initially analyzed separately. Based on the observations from structural and seismic analysis, starting conditions were now only varied in a narrow corridor around the above best fit solution. The near-surface dip of the individual faults was varied by up to ±15° about 55°E, the average fault dip measured at surface. Thrust displacement was varied between zero and 800 m as identified from seismic and surface data. The shear angle was varied by a maximum of ±10° about 90°—i.e., subvertical—as indicated by a similar number of exposed east and west dipping small faults with approximately symmetrical dip angles around a subvertical bisector. Very closely spaced faults were combined in a single fault for simplicity by summing their displacement (e.g., the two easternmost faults in the seismic line forming fault D; fault A). The section is oriented parallel to the average shortening direction derived from small-scale faults and is perpendicular to the trend of map-scale structures, resulting in an EW transect (Figure 3). The standard plane strain assumption underlying the chosen restoration algorithm appears well founded since the structures modeled are linear in plan view, because observed fault slip is consistently downdip, and because bulk deformation is small.

[37] Finally, we performed a complete sequential fault restoration to include the interaction of structures by inverting the identified westward propagating deformation, thereby using the basin filling geometries as further constraints. A key element for this final step is the initial, i.e., Oligocene, elevation of the pre-Neogene basement (Figure 2) to which the present day basement geometry has to be restored (Figure 9). Since paleoelevation is difficult to assess, we based our estimate on two lines of indirect reasoning:

[38] 1. Continuous Eocene to Miocene sedimentation in the Altiplano back arc area partly from a westerly source—

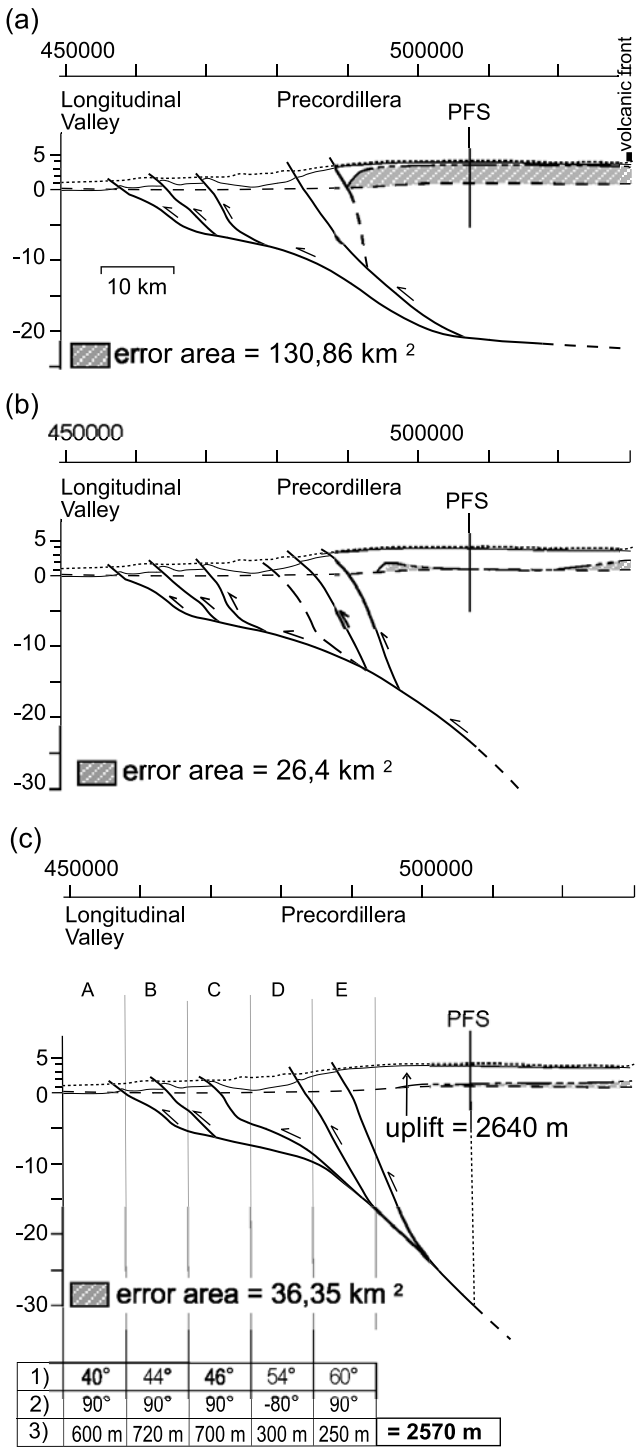

Figure 9. Deformation of basement surface at various geometries of master fault. Dashed line shows estimated original basement top (see text), thin line shows present basement top, long-short dashed line is restored basement top, and dotted line indicates present surface. Shaded area denotes error area (see text for definition). Table below best fit model in Figure 9c gives geometric values identified for optimum result for individual faults: 1, ramp angle; 2, angle of inclined shear; 3, horizontal shortening.

in the Precordillera area—has proceeded under continental conditions [*Jordan and Alonso*, 1987; *Horton et al.*, 2001]. From more coarse-grained sediments deposited in particular in the western Altiplano sedimentation developed to more fine-grained, homogeneous deposits at the end of the Oligocene and shows an increasing sediment influx from the east. The associated degradation of relief in the Precordillera area is also reflected in the modeling of the apatite fission track data by *Maksaev and Zentilli* [1999] indicating only minor difference in elevation between Precordillera and Altiplano by the Oligocene. For the middle Miocene, *Gregory-Wodzicki et al.* [1998] reconstruct sedimentation in the Altiplano to have occurred at some 1000 ± 1000 m elevation based on Paleoflora analysis. For the western Altiplano, *Muñoz and Charrier* [1996] reconstruct a paleoelevation of 1000 ± 200 m during deposition of the late Oligocene to early Miocene Chucal formation from similar arguments. For the Oligocene stage, elevation in the back arc is hence expected to have been lower than this value, but above sea level, superseded by the sediment-yielding Precordillera in the west.

[39] 2. For the latter, the elevation estimate for the Oligocene makes use of results by *Haschke and Günther* [2003] at 20°–22°S on Eocene crustal shortening of the Cretaceous-Paleogene arc constituting the Precordillera, as well as of fission track data [*Maksaev and Zentilli*, 1999]. Initial crustal thickness prior to the Eocene is estimated to some 37 km based on sedimentation above sea level (continental red beds of Cretaceous/Paleocene age grading into shallow water carbonates in the back arc to the east) and geochemical data [*Haschke and Günther*, 2003]. Observed Eocene shortening (9 km) added a minimum of 5.4 km to crustal thickness. A maximum addition of 8 km (equivalent to nearly doubling the observed shortening) is estimated from the maximum crustal thickness of 45 km allowed by geochemical data. Minimum average erosion in the Eocene/Oligocene of 1.2 ± 0.3 km was derived from the volume of eroded hanging walls of Eocene thrusts (based on the above results from *Haschke and Günther* [2003]). The maximum erosion estimate is some 4–5 km from apatite fission track data. *Maksaev and Zentilli* [1999] base this value on the assumption of a 30°C/km gradient, which probably underrates the gradient at a volcanic arc. At a standard density contrast between arc crust and mantle (2.75 versus 3.35 g/cm^3) the remaining thickness would lead to an isostatically compensated contribution to initial elevation of some 0.2–1.3 km. Considering the sum of the arguments underlying this calculation, we expect the late Oligocene elevation to have ranged between 0.7 and 2 km (identical to the present-day Patagonian Andes). For modeling we started with 1 km and explored the effect of the uncertainty.

[40] Joint modeling of the individual fault geometries underlying the plateau flank aimed at a best fit between restored and initial basement geometry and helped to explore the deep architecture of the faults. To this end, we iteratively minimized an error area defined by the area in cross section between the top of the pre-Neogene basement and the top of the restored pre-Neogene basement. Further constraints on fault geometry were defined in a second forward modeling step, in which basement geometry created by thrusts and resulting piggy back basins was tested for viability with the observed depositional geometries of the APF.

5.3. Results

[41] Forward modeling as well as direct fault trace prediction using the above constraints showed that faults A, B, and C require a ramp-flat geometry to generate the respective leading folds and thrust-top basins (Figure 8b, level 1). In all three cases, individual fault modeling resulted in a similar depth range to the detachment at some 5–8 km below sea level increasing eastward. This, and the temporal overlap of thrusting, suggests that they merge in a common detachment at this depth range. Faults D, E, and F mainly exhibit hanging wall uplift and tilting with little or no folding. This resulted in a more constant fault dip toward depth with increasing dip angles of the more eastward faults. From the age relationship of the faults, the mildly east dipping detachment linking the younger faults A-C should either crosscut these earlier, steeper, fault trajectories or merge with them to form a common detachment that steps from the upper crustal flat to a deeper crustal level across a midcrustal ramp.

[42] Joint restoration of the entire fault system shows that a bulk geometry where the individual splays all root in a subhorizontal detachment is highly unlikely (Figure 9a): Vertical uplift and tilting of the plateau margin would only be minimal resulting in an unacceptably large error area. This area is equivalent to an initial altitude in the area of the Precordillera of around 3000 m with an extremely steep western flank, both of which are not borne out by geological evidence. In order to reduce this misfit to the estimated initial elevation, faults E and F could alternatively continue linearly toward depth and provide a joint throw of some 2 km, which, however, is not borne out by field evidence.

[43] A smoothed ramp-flat-ramp geometry without a flat detachment yields a much better restoration (Figure 8c, level 1). However, the uneven distribution of the error area requires a very narrow 2000 m high bulge in the Precordillera area and a large depression close to sea level at the site of the present plateau margin. These features are also highly unlikely, because they would have prevented westward transport of the ignimbrite flows that originated from the present magmatic arc and, at the same time, would have focused deposition of very thick sedimentary infill in the depression. Since this is not observed (cf. Figures 3 and 4), we prefer a solution with a more pronounced flat-ramp transition toward depth albeit its slightly larger error area. The magnitude of the error is geometrically acceptable, and its more even lateral distribution is geologically more viable.

[44] In summary, a general splay fault geometry and an upper flat segment of the master fault are very robust features that provide a satisfactory explanation of the near surface structures and that are nearly identical in all iterations. The adjacent lower ramp, which causes large-scale regional tilting of the imbricate fan surface and uplift of the plateau,

is also a robust feature, in general, with a slightly higher uncertainty regarding its specific geometry (see below). The elevation and the subhorizontal attitude of the exposed basement top at the plateau margin with its easternmost part disappearing under the present volcanic front constrain the deep crustal ramp only down to some 30 km. Here it intersects, or merges with, the master fault of the Precordilleran fault system projected from the surface along its subvertical near-surface attitude [cf. *Reutter et al.*, 1996].

[45] Bulk horizontal shortening is found to be very small with 2500–3000 m or some 4 to 5% of the original width. Although only minor, this value entirely explains the observed structures as well as some 2600 m of surface uplift at the plateau margin at this latitude. A lower ramp dipping steeper than the here-modeled 44° best fit would even produce more surface uplift requiring less original relief. This, however, is in conflict with the above cited geological evidence for an Oligocene topographic high in the Precordillera area. Reducing the lower ramp angle, on the other hand, either requires a higher than assumed pre-Neogene elevation of this topographic high or additional mechanisms supporting surface uplift and tilting of the monocline. A ramp dip of 35° or of 25°, for example (initial elevation: 1.8 km or 2.4 km respectively), would require a mechanism generating additional uplift by 800 m or 1400 m, respectively (see also below for supporting evidence of the here-presented solution).

[46] The splay faults form a continuous fan that becomes steeper to the east (Figure 9). Shape and location of this fan match the Eocene transpressional structure responsible for the proto-Precordillera as found further south (22°–23°S) [*Maksaev and Zentilli*, 1999; *Haschke and Günther*, 2003]. Here it was shown to form a classical positive flower structure. Neogene contraction apparently reactivated some of the inclined faults, but not the subvertical master fault of the Precordilleran Fault System, probably because of its mechanically unfavorable orientation with respect to E–W directed horizontal compression. This is in contrast to sinistral motions on the PFS identified further south (22°S) for parts of the late Oligocene to middle Miocene by *Tomlinson and Blanco* [1997] that, however, did not affect the APF deposits on the plateau edge at 20°–21°S.

[47] Linking the geometric results to the above timing constraints allows deriving averaged rates of shortening and uplift. This is performed by evenly distributing the modeled shortening for each fault over its period of maximum and minimum activity respectively as estimated from crosscutting relationships and isotopic ages of affected deposits (Figure 10d). In addition, potential error in determining heave is estimated at ±10% and is used to assess the highest and lowest possible shortening rates for each fault over its activity period. Summing the components of all faults provides bulk minimum shortening rates (overestimated shortening and maximum activity period) and bulk maximum shortening rates (underestimated shortening and minimum activity period). The difference yields the uncertainty. On the basis of these data, a smoothed curve of cumulative shortening was derived (see Figure 10b). As a result, we find that average shortening rates initially reached a value of some 0.07 mm/yr in the Late Oligocene followed by an early Miocene lull in shortening rate and a distinct acceleration to a maximum of some 0.22 mm/yr in the middle Miocene (17–10 Ma) prior to subsequent slowdown. With

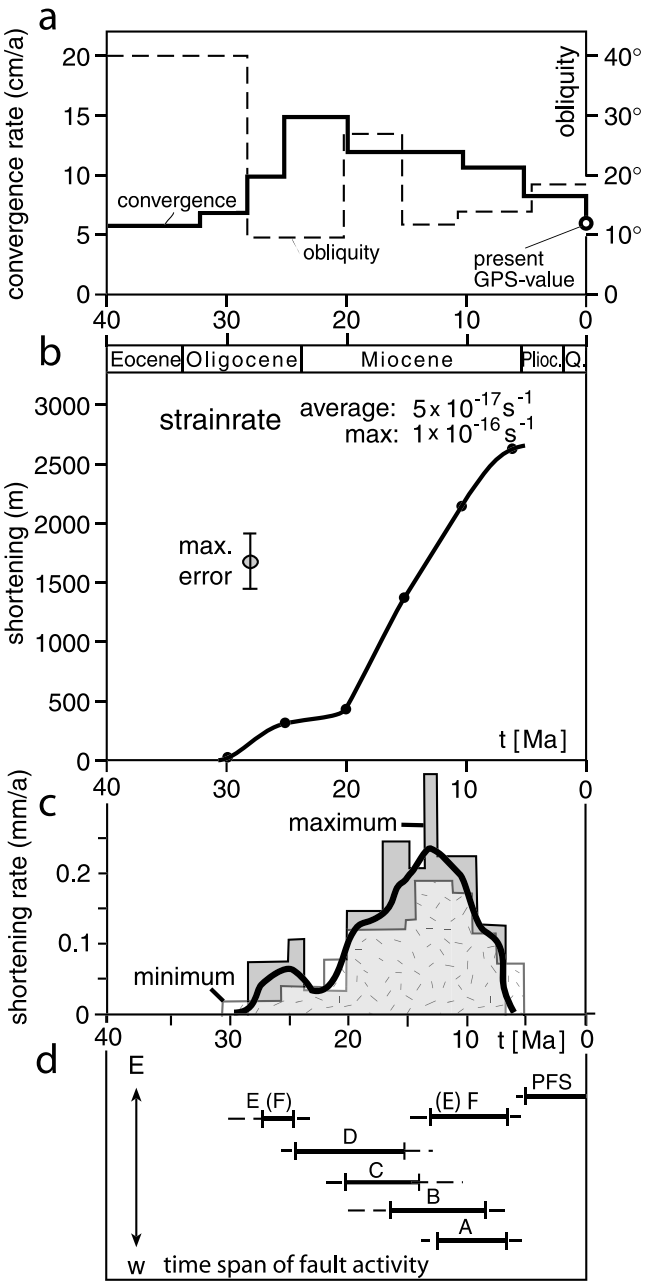

Figure 10. Evolution of shortening at Altiplano flank. (a) Plate convergence rates and obliquity between Nazca plate and South America during the Neogene (based on *Somoza* [1998]). (b) Evolution of shortening at Altiplano flank (see text for calculation strategy). (c) Shortening rates calculated from age span of associated syntectonic deposits and fault heave. Bold line depicts the preferred solution. (d) Minimum and maximum time of activity of individual faults as identified from field and seismic section analysis.

exception of the early stage, the shortening rate is partitioned on two to three of the major faults at any time increment. From these figures, Neogene strain rates in the western Altiplano were at an average of 5×10^{-17} s^{-1} with a middle Miocene maximum of 1×10^{-16} s^{-1}. The corresponding average rate of surface uplift of the plateau margin was on the same order of magnitude with some 0.1 mm/a.

6. Discussion

6.1. Fault Continuation at Depth

[48] The deep continuation of the here-described fault system and the relative contribution of fault-controlled versus flexurally controlled surface tilting can be additionally explored through integration of the results with the deep geophysical image of the Altiplano crust. The transect ANCORP'96 imaged the central Andes at 21°S with an integrated geophysical experiment that comprised reflection and wide-angle seismology, receiver-function analysis, tomography from teleseismic data, and potential field data [*ANCORP Working Group*, 1999, 2003; *Yuan et al.*, 2000]. The reflection seismic data show prominent midcrustal reflectors between 20 and 35 km depth that are consistently related to a plateau-wide *S* wave low-velocity zone (Altiplano Low-Velocity Zone (ALVZ); Figure 11a). These geophysical properties coincide spatially with the extent of Neogene to present magmatism at surface. This joint observation was interpreted as reflecting melts and metamorphic fluids that occur, in a patch-like manner, throughout most of the plateau middle crust [*Yuan et al.*, 2000; *ANCORP Working Group*, 2003].

[49] The most prominent of these bright spots, the Quebrada Blanca bright spot, underlies the study area (see Figure 11a). At surface, its boundaries are traced by the subvertical Precordilleran fault system in the west and by the recent volcanic front in the east. Interpretation suggested that the seal, which is required to prevent fluid escape, was broken at these boundaries by activity of the above structures thus destroying the potential for reflectivity [*ANCORP Working Group*, 1999]. The straight, slightly west dipping upper and lower boundaries of the bright spot are not interrupted or offset in between these two limits. In the here-presented model, the deep ramp of the fault system meets the western tip of the Quebrada Blanca bright spot at its downdip end (Figure 11a). At a shallower ramp dip between 35° and 25°, the fault should cut across the bright spot and either cause offset or create another leak, none of which are observed. Moreover, the thermal structure and lower cutoff of seismicity (only observed south of 22°) indicate that the fault reaches the brittle-plastic transition near the bright spot and the ALVZ (see Figure 11a).

[50] The role of the bright spot and the ALVZ as a potential decoupling surface, however, is unclear. Merging of the ALVZ and the west vergent fault system suggests the possibility of a subhorizontal shear zone transferring shortening eastward along a decoupling surface. If so, a major east facing backlimb of the basement top should project to the surface below the present volcanic arc. The entire Precordillera and parts of the Western Cordillera, i.e., their pre-Neogene basement, should then correspond to a crustal-scale fault-bend fold. Alternatively, the above fault system may link to the subvertical Precordilleran fault system, accommodating upper crustal shortening in a broad zone of diffuse strain at depth. In that case, the surface response would be less well constrained. In summary, the deep geophysical results lend additional support to the here-developed ramp-flat-ramp fault model and provide hints for a possible relationship between formation and localization of the fault to fluid- or melt-assisted processes in the middle crust.

6.2. Regional Extent and Correlation With Altiplano Development

[51] The west vergent fault system as identified here at 20°–21°S, is not an isolated feature (Figure 11b). *Sébrier et al.* [1988], *Muñoz and Charrier* [1996], *Farias et al.* [2002], and *García et al.* [2002] detected similar faults north of 19°30′S—up to Southern Peru. These were active between 22 and 6 Ma with a Paleogene precursor and were associated with a similarly low magnitude of shortening. At 19°S, gravitationally collapsed parts of the plateau flank postulated by *Wörner et al.* [2000], but disputed by *García and Hérail* [2001], slightly modify the monocline geometry and overprint the contractional structure, but are not responsible for uplift and formation of the monocline. Toward the south, at 22°30′S, *Haschke and Günther* [2003] reported west vergent thrust faults that expose a Cretaceous volcanic suite overthrust on continental clastics of Miocene age. Our observations between 21° and 22°S corroborate a discontinuous system of mostly west vergent faults, partly related to open folds in Neogene sediments that cover the toe of the plateau flank and are onlapped by undeformed equivalents of the Soledad Formation as farther north.

Figure 11. (a) Cross section through entire central Andean forearc and Altiplano plateau margin at 20°–21°S based on geophysical results from line ANCORP'96 and receiver function data (modified from *ANCORP Working Group* [2003]; *Yuan et al.* [2000]). QBBS is Quebrada Blanca Bright Spot; ALVZ is Altiplano Low-Velocity Zone. (b) Age distribution of ignimbrites and andesites along Altiplano flank between 18° and 24°S (data compiled from *Mortimer* [1973]; *Baker* [1977]; *Baker and Francis* [1978]; *Lahsen* [1982]; *Vergara and Thomas* [1984]; *Rutland et al.* [1965]; *Vergara et al.* [1986]; *Muñoz and Charrier* [1996]; *Wörner et al.* [2000]; *Muñoz et al.* [2002]) superimposed on time span of activity of west Altiplano fault system at various latitudes as identified here at 20°–21°S and as interpreted from published data (see below). (c) Map shows occurrence of thrust faults at flank of Altiplano as observed by various authors (1, 2 [*Muñoz and Charrier*, 1996; *García et al.*, 2002]; 3 [this paper]; 4 [*Buddin et al.*, 1993; *Haschke and Günther*, 2003]; 5 [*Jolley et al.*, 1990, *Mpodozis et al.*, 2000; *Jordan et al.*, 2002, *Muñoz et al.*, 2002]; 6 [*Kuhn*, 2002]; 7 [*Sébrier et al.*, 1988]; 8 [*Audin et al.*, 2002]).

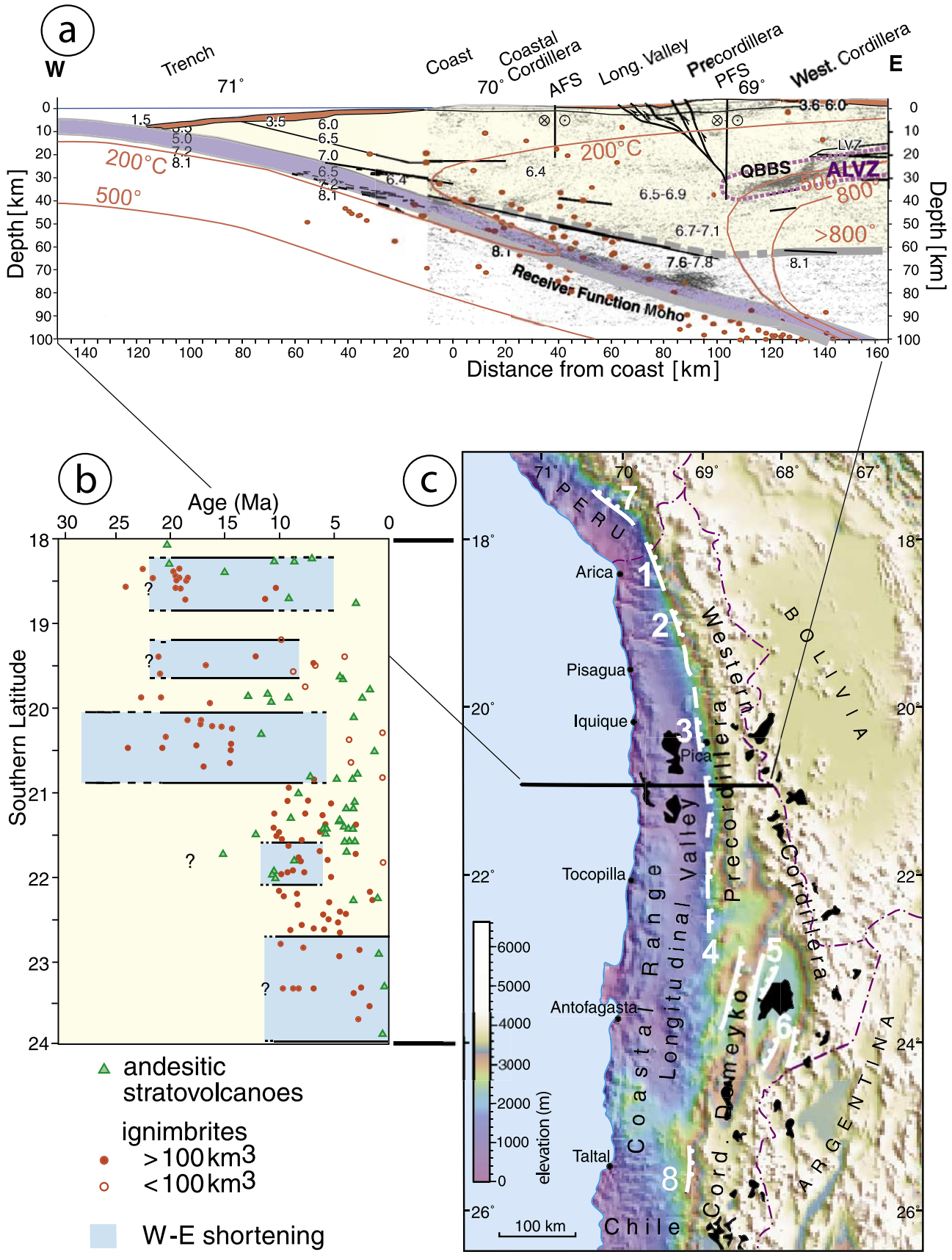
a
W
E
Trench
Coast
Coastal Cordillera
Long. Valley
Precordillera
West. Cordillera
AFS
PFS
71°
70°
69°
200°C
500°
800°
>800°
QBBS
LVZ
ALVZ
Receiver Function Moho
Depth [km]
Distance from coast [km]
b
Age (Ma)
Southern Latitude
andesitic stratovolcanoes
ignimbrites
>100 km3
<100 km3
W-E shortening
c
PERU
BOLIVIA
ARGENTINA
Chile
Arica
Pisagua
Iquique
Pica
Tocopilla
Antofagasta
Taltal
Coastal Range
Longitudinal Valley
Western Precordillera
Cord. Domeyko
elevation (m)
100 km

Figure 11

[52] Toward the Puna south of 22°S, the plateau flank acquires a more complex, laterally segmented style with a major depression separating the Cordillera Domeyko from the volcanic Western Cordillera (the Preandean depression and Salar de Atacama basin). Here, *Jolley et al.* [1990], *Mpodozis et al.* [2000], *Kuhn* [2002], *Jordan et al.* [2002], and *Muñoz et al.* [2002] report west and east vergent faults and minor contractional structures at the toe of the flanks of both Cordilleras and in the Salar. Formation of these structures has occurred during an earlier Paleogene contraction succeeded by a stage of late Miocene (circa 10–11 Ma) to recent reactivation, as indicated by ongoing upper crustal seismicity. At 25°S, *Audin et al.* [2002] found similar west vergent faults affecting a syntectonic Miocene sequence. Hence we conclude that the plateau flank between at least 17° and 23°S, possibly even further south, is associated to a similar family of contractional structures as identified here.

[53] As evidenced from the depositional record and structural relationships, surface uplift and formation of the Western Monocline was largely concluded by the end of the Miocene north of 22°S. This timing correlates with deformation of the Altiplano plateau domain and the Eastern Cordillera in the back arc. Here the main deformation is confined to between 30 and 10 Ma [*Sempere et al.*, 1990; *Gubbels et al.*, 1993; *Kennan et al.*, 1995; *Kley*, 1996] with an earlier, Paleogene, increment in the Eastern Cordillera [e.g., *Lamb and Hoke*, 1997]. The main stage of Andean contraction with shortening and underthrusting in the Subandean belt, however, only commenced in the late Miocene and persists to the present [*Baby et al.*, 1997; *Allmendinger et al.*, 1997; *Kley*, 1996] without showing any equivalent at the western flank. This clearly suggests kinematic coupling of Western Monocline formation with deformation in the plateau domain, but not with Late Neogene underthrusting in the Subandean fold and thrust belt uplifting the Eastern plateau margin (Eastern Cordillera). Last, but not least, evolution of shortening at the west Altiplano flank exhibits a complex relationship with Neogene plate convergence rates [*Somoza*, 1998]: shortening started as convergence accelerated in the Late Oligocene. According to our observations (Figure 10), however, at maximum convergence rates in the early Miocene, shortening rates dropped before accelerating during subsequent slowdown of plate convergence. This suggests an additional mechanism beyond convergence rates controlling upper plate deformation (see below).

[54] Tilting of the plateau flank and uplift of its margin has occurred relative to a virtually inert forearc that has remained largely fixed with respect to sea level during the entire Neogene (no more than 400 m vertical motion). The effect of the additional topographic load on forearc motion of more than 2.5 km generated by the thick-skinned Neogene imbrication is surprisingly small. From the axis of the Coastal Cordillera to the toe of the plateau the Oligocene Choja Pediplain currently dips by some 1°–2° east (cf. Foldout 1c and Figure 11a). Sedimentary infill of the Longitudinal Valley exhibits eastward thickening wedges. Hence the Longitudinal Valley takes the position of an underfilled foreland basin to the Altiplano flank. In order to explain this only minimal change of the basement elevation, crustal thickening under the western plateau domain must have isostatically balanced the above topographic loading. In addition, sedimentation history suggests that thickening must have occurred in the same time span as recorded for the formation of the monocline, i.e., between approximately 30 and 5 Ma. Since the here described structures only add a mere 1.5 km to the late Paleogene crustal thickness, the maintenance of isostatic equilibrium of the rising western plateau and stable forearc crust must have largely been compensated by other mechanisms of crustal thickening: These include magmatic underplating [*Haschke et al.*, 2002], and/or as yet underestimated shortening in the central parts of the plateau that was transferred westward.

6.3. Uplift of Plateau Flank and Magmatism

[55] It has been repeatedly suggested that formation of the Altiplano has a link with ignimbrite magmatism mainly based on the close spatial relationship between the occurrence of ignimbrites and plateau-style thickened crust [e.g., *Isacks*, 1988; *de Silva*, 1989; *Kay et al.*, 1994; *Francis and Hawkesworth*, 1994; *Allmendinger et al.*, 1997]. The above authors have hypothesized that this correlation indicates a significant contribution of thermal processes in initiating crustal shortening and plateau deformation. The here-reported data show that ignimbrite magmatism spans the entire period of surface uplift and shortening at the western plateau flank to the point that peak eruption intensity (24–14 Ma) correlates with the period of maximum shortening rates (Figure 11b). The available age data for ignimbrites of the Altiplano flank between 18° and 23°S as compiled from literature, moreover, show a systematic pattern along the plateau flank: Large-volume ignimbrites (>100 km^3 erupted volume) north of 21°S span the period from 25 to 10 Ma, while south of 21°S the activity of large-volume ignimbrites is bracketed between 12 and 2 Ma. Some small volume ignimbrites also occur later (see Figure 11b). Subduction-related andesite magmatism started around 13–15 Ma along the entire Altiplano flank—and only after 3 Ma at the Puna flank south of 22°S.

[56] In Figure 11b we mapped our deformation time span data at 20°30′ with those reported by other authors together with the latitudinal locations of published age data from volcanic rocks along the west flank between 18° and 24°S. Superposition yields an intriguing relation between both sets of data. The respective observed local shortening periods largely match the eruption phase of large-volume ignimbrites with exception of the Puna flank, where deformation started significantly earlier than small-volume ignimbrite magmatism. This relationship also holds for the jump in age of deformation and magmatism at the 21°S transition (Figure 11c). South of this transition, plateau uplift may be younger. This is indirectly indicated also from (1) the deflection of the drainage divide at this latitude, and (2) a slightly higher average altitude of the Precordillera with widely exposed basement to the south along with deeper valley incision and substantially higher surface

roughness indicating younger and higher uplift as compared to the north. Still further south, in the Salar de Atacama area south of 22°S, some present continuation of deformation is indicated by active seismicity below the plateau flank [*Belmonte*, 2002]. Hence the apparently continuous flank of the western Altiplano has developed diachronously in clearly defined segments, each of them largely synchronous to local ignimbrite magmatism.

[57] The correlation of deformation and surface uplift to large-volume ignimbrites suggests that the reason for this discontinuous evolution of the plateau flank in time and space must be sought in the processes controlling melt formation. Large-volume ignimbrites are, with the exception of some occurrences related to excessive mafic volcanism, commonly considered to reflect large-scale crustal melting processes [e.g., *Bryan et al.*, 2002]. This is in line with our observations from the APF ignimbrites. They are apparently not related to any mafic effusives, and the regular increase in both Sr and Nd isotopic ratios with time (Figure 5) is best explained by undisturbed radiogenic ingrowth in a crustal environment. From the correlation of initial $^{87}Sr/^{86}Sr$ ratios with extrusion ages, an apparent $^{87}Rb/^{86}Sr$ ratio of ~2 in the magma source region can be calculated, again pointing to a crustal melting environment. Similar observations were made on large-volume ignimbrites at 18°S (rhyodacitic, 23–19 Ma Oxaya ignimbrites [*Wörner et al.*, 2002]), and various younger (late Miocene to Pliocene) ignimbrites south of 21°S (ignimbrites of the Altiplano-Puna Volcanic Complex, APVC, 21°–24°S) that are considered to have involved large-scale melting in the middle crust [*Hawkesworth et al.*, 1982; *de Silva*, 1989; *Francis and Hawkesworth*, 1994; *Lindsay et al.*, 2001]. Comparison of our results with literature data for other Altiplano-Puna ignimbrites [e.g., *Hawkesworth et al.*, 1982; *Coira et al.*, 1993; *Lindsay et al.*, 2001] shows that both initial Nd ($\varepsilon_{Nd}(t)$ of −3.4 to −3.8 for APF versus ~−7 to −9 for APVC ignimbrites) and Sr ($(^{87}Sr/^{86}Sr)_i$ of ~0.7056–0.7059 versus ~0.707–0.713) indicate a distinctively prominent contribution of young (late Paleozoic-Cenozoic) juvenile additions to the crust in the source of the APF magmas (cf. primitive isotopic signatures similar to APF magmas are restricted to other ignimbrites of the Main Andean Western Cordillera [*Kay et al.*, 1999]). While some ignimbrite families of the APVC show indications for limited admixture of mantle-derived mafic magma [e.g., *Lindsay et al.*, 2001], the striking isotopic homogeneity of different APF magma batches (Figure 5), together with the evolved rhyolitic composition and the negative $\varepsilon_{Nd}(t)$ values, suggests a long-term stable intracrustal source and a long-term evolution of the magmas without significant syn-magmatic mafic additions.

[58] However, the nature of the relationship between eruption of crustal melts and active deformation is ambiguous. Melts residing within the crust may have been tapped during compressional failure of the crust, triggered for example by increased late Oligocene to Miocene convergence rates. In no case, however, have any of the thrusts in the western Altiplano so far been found to have formed conduits for melts. Rather, ignimbrite calderas were recently found to cluster close to major lineaments obliquely crossing the plateau [*Riller et al.*, 2001]. This is in line with recent findings in other orogenic belts, where mapped faults are rarely found to channel melts to the surface although both may have a more intimate relationship at depth [*Paterson and Schmidt*, 1999; *Petford et al.*, 2000, and references therein].

[59] More likely, deformation of the western Altiplano was triggered by thermal weakening due to progressive heating and melting of crust at failure equilibrium. Crossing of some critical thermal threshold associated with a critical proportion of melting in the crust might then have triggered failure in the overlying crust. Numerical modelling by *Babeyko et al.* [2002] and analytical solutions by *Watanabe et al.* [1999] clearly indicate that shortening rates are significantly enhanced by progressive crustal melting at constant stresses. Moreover, the results by *Babeyko et al.* [2002] show that crustal shortening drives melt ascent in the deeper crust. Rising melts, in turn, progressively focus upper crustal deformation above the site of midcrustal melt emplacement. This preferred interpretation is supported by the fact that failure of the western Altiplano crust occurred at the boundary between partially molten crust and a cold forearc (see Figure 11a), the expected site of a major stress and strength perturbation. Accordingly, lateral N–S variations of either the thermal state of the crust and/or its composition should be the most likely causes for the observed lateral segmentation of flank evolution and structural style, and the discontinuity in southward addition of plateau segments. Obviously, the conditions responsible for formation and advection of crustal melts from some mechanism not directly related to subduction magmatism in the Andes are a key issue requiring deeper understanding (see recent discussions on removal of mantle lithoshere by, e.g., *Allmendinger et al.* [1997, and references therein]). This is underscored by the conjecture that mechanical weakening of crust by progressive melting provides a compelling mechanism to decouple plate convergence rates and upper plate deformation rates.

7. Conclusions

[60] Following some Paleogene deformation in the arc area, the main stage of uplift of the western flank of the central Andean cordillera started in late Oligocene times, with peak rates in the middle Miocene during a stage of focused plateau development [cf. *Allmendinger and Gubbels*, 1996; *Allmendinger et al.*, 1997; *Gregory-Wodzicki et al.*, 1998; *Hindle et al.*, 2002]. North of 21°S, this process was terminated at some 7 Ma, when the zone of active shortening progressively shifted from the plateau and the eastern Cordillera into the Subandean zone [*Sempere et al.*, 1990; *Gubbels et al.*, 1993; *Kennan et al.*, 1995; *Kley*, 1996]. Uplift of the western plateau clearly evolved during an earlier stage of diffuse plateau-wide deformation and cannot be related to late Neogene underthrusting of the Brazilian shield. A compilation of tectonic and magmatic data along the plateau flank indicates a consistent set of features:

[61] 1. A west vergent prograding system of reverse faults active between some 30 and ~7 Ma is related to the

evolution of the western Altiplano flank. These faults are probably kinematically linked by an underlying east dipping master fault that plunges into the middle crust below the Precordillera. In spite of very small deformation at low strain rates, this fault system largely or totally controlled surface uplift and tilting of the western plateau margin with respect to a nearly fixed foreland in the Longitudinal Valley. No or only minor contribution to surface uplift by other mechanisms is required.

[62] 2. Ignimbrite type magmatism from a crustal source is coeval with peak activity of the western Altiplano fault system and related to uplift of this part of the plateau.

[63] 3. The western plateau flank is laterally segmented with temporally varying phases of deformation and ignimbrite magmatism while these two processes nearly always occur synchronous in each segment. Some segments started uplift as early as Oligocene (Altiplano flank) while others only started in Miocene times with some still ongoing deformation as observed in seismicity (Puna flank).

[64] 4. In several segments, subduction-related andesite magmatism only initiated close to or after the end of contractional deformation and plateau uplift and continues during the present stage of transtensional deformation of the plateau margin.

[65] The described pattern of stepwise, southward younging addition of plateau segments and their respective relationship to crustal melts clearly indicate that crustal heating and melting only locally related to subduction magmatism were key elements to initiate deformation and uplift of at least the western part of the plateau. As suggested earlier by *Isacks* [1988], thermal weakening of a critically stressed crust played a central role [cf. *Babeyko et al.*, 2002], while the conditions for crustal melting were met at different times. Moreover, the above fault system and the plateau edge appear to be localized by the boundary between hot, partially molten crust of the plateau and a colder, mechanically stronger forearc crust.

[66] **Acknowledgments.** This research was funded by GFZ Potsdam and was part of a collaborative effort with the Berlin-Potsdam Andes research program (SFB 267) and the German reflection seismic program (DEKORP). We wish to thank our Chilean colleagues, Guillermo Chong, Hans Wilke, and Gabriel Gonzalez (Universidad Catolica del Norte, Antofagasta, Chile) for the introduction to the field and many stimulating discussions. We are particularly grateful to ENAP, the Chilean national oil company, for providing the seismic and well data, which were a key element of this study. Last, but not least, we wish to thank the numerous colleagues who helped shape our ideas in repeated discussions or by providing important components or reviews of this study: M. Dziggel helped to produce some of the figures; J. Herwig contributed with age dating; T. Vietor calculated the digital topographic data in Figure 2, and M. Haschke's criticisms on an earlier draft of this manuscript provided guidance for a more readable version; finally, the thoughtful reviews by T. Jordan and R. Charrier have substantially helped to clarify a number of issues. All of this support is gratefully acknowledged.

References

Allmendinger, R. W., and T. Gubbels (1996), Pure and simple shear plateau uplift, Altiplano-Puna, Argentina and Bolivia, *Tectonophysics*, *259*, 1–13.

Allmendinger, R. W., T. E. Jordan, S. M. Kay, and B. Isacks (1997), The evolution of the Altiplano-Puna Plateau of the central Andes, *Annu. Rev. Earth Planet. Sci.*, *25*, 139–174.

Alpers, C. N., and G. H. Brimhall (1988), Middle Miocene climatic change in the Atacama Desert, northern Chile: Evidence from supergene mineralization at La Escondida, *Geol. Soc. Am. Bull.*, *100*, 1640–1656.

ANCORP Working Group (1999), Seismic reflection image revealing offset of Andean subduction-zone earthquake locations into oceanic mantle, *Nature*, *397*, 341–344.

ANCORP Working Group (2003), Seismic imaging of a convergent continental margin and plateau in the central Andes (Andean Continental Research Project 1996 (ANCORP'96)), *J. Geophys. Res.*, *108*(B7), 2328, doi:10.1029/2002JB001771.

Audin, L., G. Hérail, R. Riquelme, J. Darrozes, J. Martinod, and M. Moreira (2002), Neotectonics on the western flank of the Domeyko Cordillera and central Andean depression (northern Chile), in *Andean Geodynamics, 5th International Symposium, Toulouse, France, 16–18 Sept. 2002*, pp. 53–56, Inst. de Rech. pour le Dév. (IRD), Paris.

Babeyko, A., S. Sobolev, R. Trumbull, O. Oncken, and L. Lavier (2002), Numerical models of crustal scale convection and partial melting beneath the Altiplano-Puna Plateau, *Earth Planet. Sci. Lett.*, *199*, 373–388.

Baby, P., P. Rochat, G. Mascle, and G. Hérail (1997), Neogene shortening contribution to crustal thickening in the back arc of the central Andes, *Geology*, *25*, 883–886.

Baker, M. C. W. (1977), Geochronology of upper Tertiary volcanic activity in the Andes of north Chile, *Geol. Rundsch.*, *66*, 455–465.

Baker, M. C. W., and P. W. Francis (1978), Upper Cenozoic volcanism in the central Andes—Ages and volumes, *Earth Planet. Sci. Lett.*, *41*, 175–187.

Beck, M. (1988), Analysis of late Jurassic-Recent paleomagnetic data from active plate margins of South America, *J. S. Am. Earth Sci.*, *1*, 39–52.

Beck, S. L., G. Zandt, S. C. Myers, T. C. Wallace, P. G. Silver, and L. Drake (1996), Crustal-thickness variations in the central Andes, *Geology*, *24*, 407–410.

Belmonte, A. (2002), Krustale seismizität, struktur und rheologie der Oberplatte zwischen der Präkordilliere und dem magmatischen Bogen (22°–24°S), Ph.D. thesis, Freie Univ. Berlin, Berlin.

Bryan, S. E., T. R. Riley, D. A. Jerram, C. J. Stephens, and P. T. Leat (2002), Silicic volcanism; an undervalued component of large igneous provinces and volcanic rifted margins, in *Volcanic Rift Margins*, edited by M. A. Menzies et al., *Spec. Pap. Geol. Soc. Am.*, *362*, 97–118.

Buddin, T. S., I. G. Stimpson, and G. D. Williams (1993), North Chilean forearc tectonics and Cenozoic plate kinematics, *Tectonophysics*, *220*, 193–203.

Coira, B., J. Davidson, C. Mpodozis, and V. Ramos (1982), Tectonic and magmatic evolution of the Andes of northern Argentina and Chile, *Earth Sci. Rev.*, *18*, 303–332.

Coira, B., S. Mahlburg-Kay, and J. Viramonte (1993), Upper Cenozoic magmatic evolution of the Argentine Puna—A model for changing subduction geometry, *Int. Geol. Rev.*, *35*(8), 677–720.

de Silva, S. L. (1989), Altiplano-Puna volcanic complex of the central Andes, *Geology*, *17*, 1102–1106.

Dingman, R., and C. O. Galli (1965), Geology and groundwater resources of the Pica area, Tarapaca province, Chile, *U.S. Geol. Surv. Bull., 1189*, 100 pp.

Farias, M., R. Charrier, D. Comte, J. Martinod, L. Pinto, and G. Hérail (2002), Active Late Cenozoic flexures in the Precordillera in northern Chile: Correlations with the shallow seismic activity, and implications for the uplift of the Altiplano, *Eos Trans. AGU*, *83*(47), Fall Meet. Suppl., Abstract T51A-1136.

Francis, P. W., and C. J. Hawkesworth (1994), Late Cenozoic rates of magmatic activity in the central Andes and their relationships to continental crust formation and thickening, *J. Geol. Soc. London*, *151*, 845–854.

Galli, O. C. (1967), Pediplain in northern Chile and the Andean uplift, *Science*, *158*, 653–655.

García, M., and G. Hérail (2001), Comment on "Geochronology (^{40}Ar-^{39}Ar-, K-Ar, and He-exposure-) ages of Cenozoic magmatic rocks from northern Chile (18°–22°S): Implications for magmatism and tectonic evolution of the central Andes" by Wörner et al. (2000), *Rev. Geol. Chile*, *28*, 127–130.

García, M., G. Hérail, R. Charrier, G. Mascle, M. Fornari, and C. Perez de Arce (2002), Oligocene-Neogene tectonic evolution of the Altiplano of northern Chile (18–19°S), in *Andean Geodynamics, 5th International Symposium, Toulouse, France, 16–18 Sept. 2002*, Inst. de Rech. pour le Dév. (IRD), Paris, 235–238.

Gaupp, R., A. Kött, and G. Wörner (1999), Paleoclimatic implications of Mio-Pliocene sedimentation in the high-altitude intra-arc Lauca Basin of northern Chile, *Paleogeogr. Palaeoclimatol. Palaeoecol.*, *151*, 79–100.

Gregory-Wodzicki, K., W. McIntosh, and K. Velasquez (1998), Climatic and tectonic implications of the late Miocene Jakokkota flora, Bolivian Altiplano, *J. S. Am. Earth Sci.*, *11*, 533–560.

Gubbels, T. L., B. L. Isacks, and E. Farrard (1993), High-level surface plateau uplift and foreland development, Bolivian central Andes, *Geology*, *21*, 695–698.

Haschke, M., and A. Günther (2003), Balancing crustal thickening in arcs by tectonic vs. magmatic means, *Geology, 31*, 933–936.

Haschke, M., W. Siebel, A. Günther, and E. Scheuber (2002), Repeated crustal thickening and recycling during the Andean orogeny in north Chile (21°–26°S), *J. Geophys. Res.*, *107*(B1), 2019, doi:10.1029/2001JB000328.

Hawkesworth, C. J., M. Hamill, A. R. Gledhill, P. van Calsteren, and G. Rogers (1982), Isotope and trace element evidence for late-stage intra-crustal melting in the High Andes, *Earth Planet. Sci. Lett.*, *58*, 240–254.

Hindle, D., J. Kley, E. Klosko, S. Stein, T. Dixon, and E. Norabuena (2002), Consistency of geologic and geodetic displacements during Andean orogenesis, *Geophys. Res. Lett.*, *29*(8), 1188, doi:10.1029/2001GL013757.

Horton, B. K., B. A. Hampton, and G. L. Waanders (2001), Paleogene synorogenic sedimentation in the Altiplano plateau and implications for initial mountain building in the central Andes, *Geol. Soc. Am. Bull.*, *113*, 1387–1400.

Isacks, B. L. (1988), Uplift of the central Andean Plateau and bending of the Bolivian orocline, *J. Geophys. Res.*, *93*, 3211–3231.

James, D. E. (1971), Andean crustal and upper mantle structure, *J. Geophys. Res.*, *76*, 3246–3271.

Jolley, E. J., P. Turner, G. D. Williams, A. J. Hartley, and S. Flint (1990), Sedimentological response of an alluvial system to Neogene thrust tectonics, Atacama Desert, northern Chile, *J. Geol. Soc. London*, *147*, 769–784.

Jordan, T. E., and R. N. Alonso (1987), Cenozoic stratigraphy and basin tectonics of the Andes Mountains, 20–28° south latitude, *AAPG Bull.*, *71*, 49–64.

Jordan, T. E., N. Muñoz, M. Hein, T. Lowenstein, L. Godfrey, and J. Yu (2002), Active faulting and folding without topographic expression in an evaporite basin, Chile, *Geol. Soc. Am. Bull.*, *114*, 1406–1421.

Kay, S., B. Coira, and J. Viramonte (1994), Young mafic back arc volcanic rocks as indicators of continental lithospheric delamination beneath the Argentine Puna plateau, central Andes, *J. Geophys. Res.*, *99*, 24,323–24,339.

Kay, S. M., C. Mpodozis, and B. Coira, (1999), Neogene magmatism, tectonism, and mineral deposits of the central Andes (22° to 33°S latitude), in *Geology and Ore Deposits of the Central Andes*, edited by B. J. Skinner, *Spec. Publ. SEPM Soc. Sediment. Geol.*, *7*, 27–59.

Keller, E. A., and N. Pinter (2002), *Active Tectonics: Earthquakes, Uplift, and Landscape*, 2nd ed., Prentice-Hall, Old Tappan, N. J.

Kennan, L., S. Lamb, and C. Rundle (1995), K-Ar dates from the Altiplano and Cordillera Oriental of Bolivia: Implications for Cenozoic stratigraphy and tectonics, *J. S. Am. Earth Sci.*, *8*, 163–186.

Kley, J. (1996), Transition from basement-involved to thin-skinned thrusting in the Cordillera Oriental of southern Bolivia, *Tectonics*, *15*, 763–775.

Kley, J., and C. R. Monaldi (1998), Tectonic shortening and crustal thickness in the central Andes: How good is the correlation, *Geology*, *26*, 723–726.

Kuhn, D. (2002), Fold and thrust belt structures and strike-slip faulting at the SE margin of the Salar de Atacama basin, Chilean Andes, *Tectonics*, *21*(4), 1026, doi:10.1029/2001TC901042.

Lahsen, A. (1982), Upper Cenozoic volcanism and tectonism in the Andes of northern Chile, *Earth Sci., Rev.*, *18*, 285–302.

Lamb, S., and L. Hoke (1997), Origin of the high plateau in the central Andes, Bolivia, South America, *Tectonics*, *16*, 623–649.

Lamb, S., L. Hoke, I. Kennan, and J. Dewey (1997), Cenozoic evolution of the central Andes in Bolivia and northern Chile, in *Orogeny Through Time*, edited by J.-P. Burg and M. Ford, *Geol. Soc. Spec. Publ.*, *121*, 237–264.

Lindsay, J. M., A. K. Schmitt, R. B. Trumbull, S. L. de Silva, W. Siebel, and R. Emmermann (2001), Magmatic evolution of the La Pacana Caldera system, central Andes, Chile: Compositional variation of two cogenetic, large-volume felsic ignimbrites, *J. Petrol.*, *42*(3), 459–486.

Ludwig, K. R. (1999), Isoplot/Ex Ver. 2. 06: A geochronological toolkit for Microsoft Excel, *Spec. Publ. 1a*, Berkeley Geochronol. Cent., Berkeley, Calif.

MacFadden, B. J., F. Anaya, and C. Swisher III (1995), Neogene paleomagnetism and oroclinal bending of the central Andes of Bolivia, *J. Geophys. Res.*, *100*, 8153–8167.

Maksaev, V. (1978), Cuadrangulo Chitigua y sector occidental del cuadrangulo Cerro Palpana, *Carta Geol. Chile*, *31*.

Maksaev, V., and M. Zentilli (1999), Fission track thermochronology of the Domeyko Cordillera, northern Chile: Implications for Andean tectonics and porphyry copper metallogenesis, *Explor. Min. Geol.*, *8*, 65–89.

Merrits, D., and K. R. Vincent (1989), Geomorphic response of coastal streams to low, intermediate and high rates of uplift, Mendocino triple junction region, northern California, *Geol. Soc. Am. Bull.*, *101*, 1373–1388.

Mortimer, C. (1973), The Cenozoic history of the southern Atacama desert, Chile, *J. Geol. Soc. London*, *129*, 505–526.

Mortimer, C., and N. Saric (1975), Cenozoic studies in northernmost Chile, *Geol. Rundsch.*, *64*, 395–420.

Mpodozis, C., N. Blanco, T. Jordan, and M. C. Gardeweg (2000), Estratigrafia y deformacion del Cenozoico tardio en la region norte de la cuenca del Salar de Atacama: La zona de Vilama-Pampa Vizcachitas, paper presented at IX Congreso Geológico Chileno, Serv. Nac. de Geol. y Min., Puerto Varas, Chile.

Muñoz, N., and R. Charrier (1996), Uplift of the western border of the Altiplano on a west-vergent thrust system, northern Chile, *J. S. Am. Earth Sci.*, *9*, 171–181.

Muñoz, N., R. Charrier, and T. Jordan (2002), Interactions between basement and cover during the evolution of the Salar de Atacama Basin, northern Chile, *Rev. Geol. Chile*, *29*, 55–80.

Naranjo, J. A., and R. Paskoff (1985), Evolucion cenozoica del piedmonte Andino en la Pampa del Tamarugal, norte del Chile, 18°–21°S, paper presented at IV Congreso Geologico Chileno, Univ. Católica del Norte, Antofagasta, Chile.

Pardo-Casas, F., and P. Molnar (1987), Relative motion of the Nazca (Farallon) and South American plates since Late Cretaceous times, *Tectonics*, *6*, 233–248.

Paterson, S. R., and K. L. Schmidt (1999), Is there a close spatial relationship between faults and plutons?, *J. Struct. Geol.*, *21*, 1131–1142.

Petford, N., A. R. Cruden, K. J. W. McCaffrey, and J. L. Vigneresse (2000), Granite magma formation, transport and emplacement in the Earth's crust, *Nature*, *408*, 669–673.

Randall, D. E., G. K. Taylor, and J. Grocott (1996), Major crustal rotations in the Andean margin: Palaeomagnetic results from the Coastal Cordillera of northern Chile, *J. Geophys. Res.*, *101*, 783–798.

Reijs, J., and K. McClay (1998), Salar Grande pull-apart basin, Atacama Fault System, northern Chile, in *Continental Transpressional and Transtensional Tectonics*, edited by R. E. Holdsworth, R. A. Strachan, and J. F. Dewey, *Geol. Soc. Spec. Publ.*, *135*, 127–141.

Reutter, K. J., E. Scheuber, and P. J. Wigger (Eds.) (1994), *Tectonics of the Southern Central Andes: Structure and Evolution of an Active Continental Margin*, Springer-Verlag, New York.

Reutter, K. J., E. Scheuber, and G. Chong (1996), The Precordilleran fault system of Chuquicamata, northern Chile: Evidence for reversals along arc-parallel strike-slip faults, *Tectonophysics*, *259*, 213–228.

Riller, U., I. Petrinovic, J. Ramelow, M. Strecker, and O. Oncken (2001), Late Cenozoic tectonism, collapse caldera and plateau formation in the central Andes, *Earth Planet. Sci. Lett.*, *188*, 299–311.

Rowan, M. G., and R. Kligfield (1989), Cross section restoration and balancing as aid to seismic interpretation in extensional terranes, *AAPG Bull.*, *73*, 955–966.

Rutland, R. W. R. (1971), Andean orogeny and ocean floor spreading, *Nature*, *233*, 252–255.

Rutland, R. W. R., J. E. Guest, and R. L. Grasty (1965), Isotopic ages and Andean uplift, *Nature*, *208*, 677–678.

Scheuber, E., and A. M. Andriessen (1990), The kinematic and geodynamic significance of the Atacama fault zone, northern Chile, *J. Struct. Geol.*, *12*, 243–257.

Scheuber, E., and G. Gonzalez (1999), Tectonics of the Jurassic-Early Cretaceous magmatic arc of the north Chilean Coastal Cordillera (22°–26°S): A story of crustal deformation along a convergent plate boundary, *Tectonics*, *18*, 895–910.

Scheuber, E., and K. J. Reutter (1992), Magmatic arc tectonics in the central Andes between 21° and 25°, *Tectonophysics*, *205*, 127–140.

Scheuber, E., T. Bogdanic, A. Jensen, and K. J. Reutter (1994), Tectonic development of the North Chilean Andes in relation to plate convergence and magmatism since the Jurassic, in *Tectonics of the Southern Central Andes*, edited by K.-J. Reutter, E. Scheuber, and P. Wigger, pp. 121–139, Springer-Verlag, New York.

Sébrier, M., J. L. Mercier, J. Machare, D. Bonnet, J. Cabrera, and J. L. Blanc (1988), State of stress in an overriding plate situated above a flat slab: The Andes of central Peru, *Tectonics*, *7*, 895–928.

Sempere, T., G. Hérail, J. Oller, and M. G. Bonhomme (1990), Late Oligocene-early Miocene major tectonic crisis and related basins in Bolivia, *Geology*, *18*, 946–949.

Somoza, R. (1998), Updated Nazca (Farallon)-South America relative motions during the last 40 My: Implications for mountain building in the central Andean region, *J. S. Am. Earth Sci.*, *11*, 211–215.

Tomlinson, A. J., and N. Blanco (1997), Structural evolution and displacement history of the West Fault System, Precordillera, Chile: Part 2, Postmineral history, paper presented at VIII Congreso Geológico Chileno, Univ. Católica del Norte, Antofagasta, Chile.

Tosdal, R. M., A. H. Clark, and E. Farrar (1984), Cenozoic polyphase landscape and tectonic evolution of the Cordillera Occidental, southernmost Peru, *Geol. Soc. Am. Bull.*, *95*, 1318–1332.

Turner, F. J. (1955), Nature and dynamic interpretation of deformation lamellae in calcite of three marbles, *Am. J. Sci.*, *251*, 276–291.

Vergara, H. L., and A. L. Thomas (1984), Hoja Collacagua, 1:250000, *Carta Geol. Chile*, *59*.

Vergara, M., C. Marangunic, H. Bellon, and R. Brousse (1986), Edades K-Ar de las ignimbritas de las Quebradas Juan de Morales y Sagasca, norte de Chile, *Ser. Comun. Dep. Geol., Fac. Cienc. Fis. Mat. Univ. Chile*, *36*, 1–7.

Watanabe, T., T. Koyaguchi, and T. Seno (1999), Tectonic stress controls on ascent and emplacement of magmas, *J. Volcanol. Geotherm. Res.*, *91*, 65–78.

White, N. J., J. A. Jackson, and D. P. McKenzie (1986), The relationship between the geometry of normal faults and that of the sedimentary layers in their hanging walls, *J. Struct. Geol.*, *8*, 897–909.

Wigger, P., et al (1994), Variations of the crustal structure of the Southern central Andes deduced from seismic refraction investigations, in *Tectonics of the Southern Central Andes*: *Structure and Evolution of an Active Continental Margin*, edited by K.-J. Reutter, E. Scheuber, and P. J. Wigger, pp. 23–48, Springer-Verlag, New York.

Wörner, G., K. Hammerschmidt, F. Henjes-Kunst, J. Lezaun, and H. Wilke (2000), Geochronology (^{40}Ar-^{39}Ar-, K-Ar, and He-exposure-) ages of Cenozoic magmatic rocks from northern Chile (18°–22°S): Implications for magmatism and tectonic evolution of the central Andes, *Rev. Geol. Chile*, *27*, 205–240.

Wörner, G., D. Uhlig, I. Kohler, and H. Seyfried (2002), Evolution of the West Andean Escarpment at 18°S (N. Chile) during the last 25 Ma: Uplift, erosion and collapse through time, *Tectonophysics*, *345*, 183–198.

Yuan, X., S. V. Sobolev, R. Kind, O. Oncken, and Andes Siesmology Group (2000), New constraints on subduction and collision processes in the central Andes from P-to-S converted seismic phases, *Nature*, *408*, 958–961.

Zandt, G., A. A. Velasco, and S. L. Beck (1994), Composition and thickness of the southern Altiplano crust, Bolivia, *Geology*, *22*, 1003–1006.

J. Glodny and O. Oncken, GeoForschungsZentrum Potsdam, Telegrafenberg, D-14473 Potsdam, Germany. (glodnyj@gfz-potsdam.de; oncken@gfz-potsdam.de)

P. Victor, Institut für Geologie, Universität Hannover, Callinstrasse 30, D-30167 Hannover, Germany. (p.victor@geowi.uni-hannover.de)